RAIRO-Oper. Res. 60 (2026) 1233–1267
https://doi.org/10.1051/ro/2026025

RAIRO Operations Research
www.rairo-ro.org

PERFORMANCE EVALUATION OF LTE DRX IN 5G BEAMFORMING WIRELESS NETWORKS: A QUEUEING MODEL APPROACH

B. Krishna Kumar[1,*], R. Navaneetha Krishnan[2], R. Sankar[2] and K. Sethukumarasamy[1]

Abstract. The rapid advancement of wireless mobile technology enables user equipment (UE) to process vast amount of data transmission. However, since wireless communication UEs are battery-powered, they require an extended operational lifespan. These battery-operated devices gradually deplete their energy with prolonged usage. To optimize energy consumption, the Long-Term Evaluation (LTE) standard incorporates a discontinuous reception (DRX) mechanism, significantly extending UE battery life in modern fifth-generation (5G) wireless networks. 5G-DRX networks utilize millimeter-wave (mmWave) frequency bands to achieve high-speed data transmission. However, mmWave transmissions require beamforming techniques to compensate for high isotropic path loss. This article proposes a Markovian queue tailored for the 5G-DRX wireless deployment, integrating a beam search-based policy to accommodate dynamic short and long sleep cycles. By incorporating queueing analysis with sleep cycles in the 5G-DRX beam searching wireless system, both UE energy efficiency and data packet delay are effectively assessed. Analytical results are derived for the transient and steady-state probabilities of UE status, considering the 5G-DRX beam alignment tracking capability and the average number of data packets queued in the buffer at the evolved Node B (eNB). Several essential queueing performance metrics are determined. Additionally, UE energy efficiency and consumption in a stationary regime are analyzed to provide valuable numerical insights.

Mathematics Subject Classification. 60K25, 60J27, 90C40, 90B22.

Received May 7, 2025. Accepted February 20, 2026.

1. Introduction

In the rapidly evolving mobile communication and computing systems, energy-efficiency and the quality of data packet transmission are two critical factors. To handle the rapid increase in mobile traffic for UE, it is crucial to maintain high data rates. In response, the 3GPP standard has introduced the mmWave spectrum in 5G radio networks, spanning from 30 GHz to 300 GHz, to meet the demand of high frequency data packet transfers [16]. By utilizing the unused high frequency band, mmWave communication can meet the high transmission

Keywords. DRX, 5G mmWave, beamforming, power saving, throughput, latency, first-passage time.

[1] Department of Mathematics, School of Advanced Sciences, Vellore Institute of Technology, Chennai 600127, India.
[2] Department of Mathematics, Vel Tech Rangarajan Dr. Sagunthala R&D Institute of Science and Technology, Chennai 600062, India.
*Corresponding author: drbkkumar@hotmail.com

rate requirements of the 5G network [49, 58]. Thus, mmWave frequencies are vital components in 5G wireless networks, enhancing throughput and enabling support for battery-powered UEs [56].

Nevertheless, the use of the mmWave frequencies in 5G wireless communication requires directional beamforming to mitigate propagation and penetration losses. Furthermore, the beam searching mechanism not only addresses the challenges of mmWave propagation but also minimizes interference while enhancing the signal strength for the UE [1]. The primary objectives of beamforming are to establish a reliable link between the eNB and the UE, ensuring seamless communication while identifying the optimal beam pair [39].

In the 5G directional air interface, however, beam tracking operations, combined with high-order modulation schemes can drain the UE's battery power. To address this issue, LTE, a widely adopted wireless communication standard, introduced the DRX protocol to enhance energy efficiency at the UE [14, 63]. Components operating during long and short sleep cycles, when there are no downlink data packets in the eNB's buffer or the UE has not received a data packet for an extended period, help reduce energy consumption. In other words, LTE DRX allows the UE to transition from an active state to short or long sleep cycles, during which period it consumes minimum energy/power when no data packets are received (see Lin *et al.* [30]).

During the DRX sleep cycles, the UE is unable to transmit the data packets but can only monitor the eNB's buffer *via* the beam tracking protocol. If any new data packets arrive during the scheduled sleep cycle, they will be buffered at the eNB. The stored packets will be transmitted only after the completion of the sleep cycle, utilizing the best beamforming pair event as defined by the LTE DRX protocol in the 5G system. Thus, it is evident that the DRX mechanism in the LTE conserves the UE's energy, but it results in additional delay in data transmission.

Numerical and analytical studies have been published in the literature that examine the performance metrics for the UE focusing on the operation of the LTE DRX scheme. By applying Markov or semi-Markov models, researchers can determine the system's stationary distribution and steady-state performance metrics after calculating the state transition probabilities. However, the majority of researchers have primarily focused on studying LTE DRX configured wireless networks using exclusively semi-Markov models (see [2, 4, 13, 14, 19, 23, 27, 31, 33–36, 38, 41, 42, 44, 45, 48, 51, 53, 55, 60, 62]).

Although the semi-Markov models have been widely used in LTE DRX networking systems, performance measures such as throughput, power-saving factor, data packet latency and first-passage time (FPT) analysis, among others, are not evaluated as effectively as in more complex Markovian models, particularly when relying on queueing analysis. Furthermore, the existing studies indicate that the Markov queueing model provides better energy-saving performance for the UE compared to the semi-Markov model [11].

The significance of queueing analysis and models as essential tools for assessing LTE DRX wireless communication has been highlighted, especially concerning energy conservation for the UE and the buffering delay experienced by the data packets at the eNB. As a result, it can be argued that studies on LTE DRX in 5G beam-form scenarios should incorporate queueing models. A few studies have explored queueing models for LTE DRX wireless networks, concentrating on the trade-off between energy consumption at the UE and the average queueing delay.

For instance, Yang and Lin [59] introduced a modified non-Markovian queue with vacation to assess the performance of Universal Mobile Telecommunications System (UMTS) under the DRX cycle. Zhu *et al.* [64] discussed a queueing model for sleep-based power-saving wireless networks, analyzing data packet delays during both sleep and active cycles. Baek and Choi [5] proposed an efficient sleep mode operation employing a non-Markovian queueing system to evaluate average data packet delays and mean power consumption of the UE. Subsequently, Baek and Choi [6] further analyzed DRX in 3GPP LTE using a discrete-time queue, considering both downlink and uplink traffic flows. Mancuso and Alouf [37] examined the downlink data packet queue behavior for the UE under the DRX protocol, exploring the characteristics of an inhomogeneous vacation queue during both busy and idle periods. Their finding demonstrated that consistent power savings could be achieved in DRX wireless access networks.

Zhang *et al.* [61] developed a discrete-time queueing model to optimize energy savings for the active DRX, where the system transitions from a working mode to a sleep mode. The analyzed performance measures include

energy consumption and the average latency of data packets. In Dimitriou [12], the impact of DRX parameters, the UE failure rate, the wireless link error rate and checkpoint overhead on metrics such as data packet delay time, and energy efficiency was investigated using a variant of non-Markovian queueing analysis. A queueing system under dynamic channel control, workload control and delivery deadlines for data packets in wireless interface networks was discussed by Lim *et al.* [29]. Additionally, they derived the mean cycle time length and the expected energy expenditure of the UE during the cycle.

Herreria-Alonso *et al.* [17] discussed a promising DRX scheme for a wireless communication network that enhances the battery lifetime of the UE while simultaneously maintaining the average data packet delay within the desired limit. In Ramazanali and Vinel [46, 47], novel queueing models were developed to estimate the power saving factor and the average queueing delay for the DRX scheme wireless network. Kawser *et al.* [20] used queueing analysis to examine the trade-off between power saving and data packet queueing delay for non-real time traffic in the LTE wireless networking system with long and short DRX sleep cycles. Li and Lo [28] proposed a traffic regulation and time slicing scheme at the eNB for the LTE DRX networking system, based on a queueing model to effectively reduce the power consumption of the UE.

Anapam *et al.* [3] have discussed a batch arrival vacation queue with N-policy for the LTE DRX communication network. The study investigates guidelines for selecting the optimal values of N and the maximum number of DRX cycles. Kempa *et al.* [21] have analyzed the trade-off between energy consumption and the number of lost data packets by treating the DRX mechanism in wireless networks as a finite-capacity vacation queue. Lokesh *et al.* [32] proposed analytical models to assess DRX-based energy efficiency of UEs in 5G heterogeneous networks. Utilizing two-dimensional CTMC and semi-Markov models, they have demonstrated notable enhancement in the system performance across user-and network-level parameters. Recently, Ruiz-Guirola *et al.* [50] have investigated a Markovian DRX mechanism aimed at reducing the energy consumption of Industrial Internet of Things (IIoT) devices under Poisson and burst traffic conditions. Their findings revealed that appropriately restarting the inactive timer can significantly enhance power savings. Specifically, they proposed a dynamic configuration method for DRX parameters to maximize energy efficiency.

All of the communication network research articles mentioned above which utilize queueing theory, emphasize steady-state results for LTE DRX wireless networks, with or without a beam searching protocol. However, the assumptions required to derive these steady-state results are rarely achieved in real-world scenarios. As a result, relying solely on the steady-state outcomes is often insufficient for applying queueing analysis in the design and evaluation of real-time LTE DRX in 5G beam tracking wireless networks.

For instance, LTE DRX wireless networks governed by the mmWave beam searching protocol experience frequent changes in network state, as mmWave beamforming controllers adjust paths to optimize beam tracking duration and energy consumption. These frequent changes suggest that, instead of operating in a steady-state regime, wireless access networks are more likely to be in transient states. As a result, the analytic transient analysis presented in this research article helps us to understand the state of the UE in the LTE DRX wireless communication system at any given time instant t. Evidently, the transient analyses offer a more realistic approach to investigating the performance of the wireless communication networks. Table 1 presents a comparison of the proposed research results with existing studies in the literature.

Motivated by these insights, this article presents exact analytical expressions for transient state probabilities and various vital time-dependent performance metrics for the UE operating under the LTE DRX in a 5G beamforming wireless network. The approach integrates queueing theory, Laplace transforms and continued fraction techniques, resulting in a sophisticated yet unconventional methodology. The derived time-dependent characteristics offer a unique and valuable contribution to the literature on LTE DRX in 5G beamforming wireless networks. Our analytic results are accurate in evaluating the energy consumption and hence provide potential guidance in efficiently managing energy. To the best of our knowledge, previous research on 5G beam tracking wireless communication has not included such a detailed time-dependent analysis.

In short, the significance and contributions of this research paper can be summarized as follows:

– A queueing model has been developed to analyze the transmission of data packets and the resulting buffer delays at the eNB in a 5G LTE DRX beamforming wireless system.

- The continued fraction technique is employed to evaluate the UE's battery life and the system throughput based on the DRX beam searching process.
- To study the dynamics of the real-time system, analytical expressions are derived for the transient probabilities of the UE states and for the virtual waiting time of data packets in the eNB buffer.
- This research also examines the FPT probability density function to analyze the transition to the long sleep state and its related features.
- For the first time, the steady-state probabilities of the UE's different states and the system's regeneration cycle are derived from the transient analysis.
- Vital performance metrics, such as 5G-DRX energy efficiency and energy consumption, are evaluated in the steady-state regime.
- Sensitivity analysis and graphical visualization of key 5G-DRX parameters are conducted to examine their impact on system performance metrics in the proposed 5G LTE DRX stochastic model for both transient and steady-state regimes.

The structure of the present article is as follows: Section 2 provides the technical background on the potential queueing processes associated with LTE DRX in a 5G beam tracking wireless system. Section 3 presents detailed analytic expressions for the transient probabilities related to the status of the UE and the average number of data packets stored in the eNB buffer, capturing the system's time-dependent behavior. In Section 4, we determine the complementary cumulative distribution function and the virtual delay of data packets under the LTE DRX mechanism in a 5G beamforming scenario at any specific time. Section 5 focuses on the FPT probability density function, specifically for reaching the long sleep period, along with its associated characteristics. Section 6 discusses the steady-state probabilities of various statuses and the regenerative cycle of the UE under an ergodic condition. Section 7 derives key steady-state performance metrics for the system under discussion. Section 8 presents vital performance indicators, such as energy efficiency and energy consumption factors for the UE. Section 9 investigates the time required to reach the level of congestion in the eNB's packet buffer. A comprehensive numerical and sensitivity analysis is also provided to better understand the LTE DRX beam searching operation in the 5G wireless communication network. The final section concludes with remarks and outlines plans for further research.

Before conducting the system analysis, the notations and descriptions are presented in Table 2.

2. Queueing dynamics in 5G-DRX wireless system

The fifth-generation (5G) mmWave communication networks are anticipated to handle high-frequency data packet rates for various types of wireless traffic. To attain these high-frequency data packet rates and enhance network throughput, the 5G wireless network utilizes a beam searching operation to identify and align the optimal beam pair before initiating seamless communication. However, during the beam searching process and the use of higher modulation techniques in the 5G wireless network, the battery power consumption of the UE is significantly high. To analyze the performance of such networks, we derive analytical expressions for the average waiting time of data packets, energy consumption, and energy saving efficiency of the UE under the LTE DRX mechanism based on a Markovian queueing model. By making use of the explicit analytical queueing performance metrics, one can focus on reducing power consumption while minimizing data packet delay for the DRX in 5G mmWave wireless networks integrating potential beam tracking techniques. Specifically, this queueing approach enables the dynamic adjustment of both short and long sleep cycles, thereby allowing us to precisely assess the latency and the congestion level of data packets in the buffer of the eNB, which serves as the central hub of the wireless networks.

The following DRX operating parameters are used in the current analyses to ensure efficient power management for the UE in the 5G wireless network:

- **Active/Busy state:** In this state, the UE monitors the downlink control channel to receive data packets from the eNB's buffer. This is an energy-intensive state where the UE is fully active and ready to transmit each data packet *via* the downlink transmitter.

TABLE 1. Comparison of related research results with our proposed work.

References	LTE	LTE-A	LTE-5G	Energy consumption	Energy efficiency	Delay	Transient analysis	Analytical/Simulation
Huang *et al.* [18]	–	✓	–	✓	✓	✓	–	Simulation
Zhang *et al.* [61]	✓	–	–	✓	–	✓	–	Embedded Markov Chain
Herreria-Alonso *et al.* [17]	✓	✓	–	–	✓	✓	–	$M/G/1$ queue with multiple vacation
Ramazanali and Vinel [47]	✓	✓	–	✓	✓	✓	–	Markov queueing model
Memon *et al.* [39]	–	–	✓	–	✓	✓	–	Simulation
Maheshwari *et al.* [36]	✓	–	✓	✓	–	✓	–	Semi-Markov
Huang *et al.* [19]	✓	–	✓	✓	–	✓	–	Semi-Markov
Anapam *et al.* [3]	–	✓	–	–	✓	✓	–	$M^X/G/1$ queue with multiple vacation
Philip and Malarkodi [42]	✓	✓	✓	✓	–	✓	–	Semi-Markov
Aghdam *et al.* [2]	✓	–	✓	–	✓	✓	–	Semi-Markov
Kempa *et al.* [21]	✓	–	–	–	–	✓	✓	$M^X/G/1/B$-type queue/Simulation
Dharmaraja *et al.* [11]	✓	–	–	✓	–	✓	✓	Semi-Markov and CTMC queueing model
Maheshwari *et al.* [35]	–	✓	✓	✓	–	✓	–	queuing model Semi-Markov
Lokesh *et al.* [32]	✓	✓	✓	✓	✓	✓	–	Markov chain and Semi-Markov
Ruiz-Guirola *et al.* [50]	–	✓	–	✓	–	✓	–	Semi-Markov
Rastogi *et al.* [48]	✓	–	✓	✓	✓	✓	–	Semi-Markov
Proposed study	✓	–	✓	✓	✓	✓	✓	CTMC queueing model

– **Short-sleep state:** A short-sleep state is a brief period designed to conserve the UE's energy by powering down its transceiver components. During this time, the UE neither transmits nor monitors the eNB's buffer. The short-sleep period is repeated for a preset random duration if no packet activity is observed; otherwise, it ends.
– **Beam searching state:** The UE enters this state after completing a short-sleep cycle, the UE measures reference signals from the available beam to align the beam pair between the UE and the eNB. During the beam forming processes, if the UE receives a notification of a new data packet, it will wait for the process to complete before transitioning to the active period to begin transmitting data packets from the buffer. If no data packet activity is detected in the eNB's buffer at the start of the beam searching period, and the short-sleep cycle expires, the UE will transition to the long-sleep state.
– **Long-sleep state:** The duration of the long-sleep state is assumed to be an integer multiple of the short-sleep period, making it longer than the short-sleep period. During the long sleep state, incoming data packets are buffered but cannot be transmitted. After completing the long-sleep cycle, if the buffer contains at least one data packet, the UE begins aligning the optimal beam pair and transitions back to the active state.

To investigate the LTE DRX in 5G beamforming technology, we model it based on a Markovian FCFS queueing system. For this scenario, we assume that downlink packets arrive at the infinite capacity buffer of the eNodeB (eNB) for the UE according to a Poisson process with rate λ and the transmission time for each packet

TABLE 2. List of notations and descriptions.

Notation		Descriptions
λ	:	Data packet arrival rate
μ^{-1}	:	Mean transmission time for each packet
δ^{-1}	:	Mean dwell time in the short-sleep state
ξ^{-1}	:	Mean dwell time in the long-sleep state
ν^{-1}	:	Mean sojourn time in the beamforming state before transitioning to the short-sleep state
η^{-1}	:	Mean sojourn time in the beamforming state before transitioning to the long-sleep state
S	:	Short-sleep state
L	:	Long-sleep state
B	:	Beamforming state
A	:	Active state
ϕ_{cycle}	:	DRX regenerative cycle length
ϕ_A	:	DRX active duratioin
ϕ_S	:	DRX short-sleep duration
ϕ_L	:	DRX long-sleep duration
ϕ_B	:	DRX beamforming duration
$f^*(s)$	:	Laplace transform of $f(t)$
$f(t) \copyright g(t)$	:	Convolution of $f(t)$ and $g(t)$
$f^{\copyright(n)}(t)$	:	n-fold convolution of $f(t)$ with itself
ρ	:	$\frac{\lambda}{\mu}$ traffic intensity
N_s	:	Number of packets transmitted during active period
N	:	Threshold level of packets in the buffer
λ_{eff}	:	Effective arrival rate
U	:	System throughput
Ω	:	Set of possible states
Ω_F	:	Set of finite states
P_n	:	Steady-state probability of being in a state n
P_{EC}	:	Mean energy consumption
P_{EE}	:	Mean energy efficiency

follows an exponential distribution with a mean of $\frac{1}{\mu}$. To improve energy efficiency in the UE while minimizing the average packet delay in the proposed DRX system, a beam-searching operation is implemented between the short-sleep and long-sleep periods. The objective of beam aligning is to establish a link between the UE and eNB, and locate the optimal beam pair. The dwell times of the UE in the short-sleep (S) and long-sleep (L) states are independent and follow exponential distributions with parameters δ and ξ, respectively. In the beamforming (B) state, if no new packet transmission takes place, the UE's sojourn time in this state before transitioning to either the short-sleep (S) state or the long-sleep (L) state follows exponential distributions with parameters ν and η, respectively. In contrast, if any new downlink data packet information is received at the start of the beam alignment period, the UE will transition to the busy/active (A) state upon identifying the optimal beam pair. As a result, whenever the UE is in an active state, it begins transmission of available data packets from the buffer through the downlink control channel until the buffer at the eNB is emptied. Once the busy/active period ends, the UE goes back to the short-sleep cycle. If no new transmission occurs in the beam-searching state and the DRX short-sleep cycle expires, the UE switches to the long-sleep cycle. After the UE wakes up from the long-sleep period, returning to the beam-tracking state is crucial for beam alignment. Consequently, from the beam searching state, the UE transitions to either the active period or returns to the

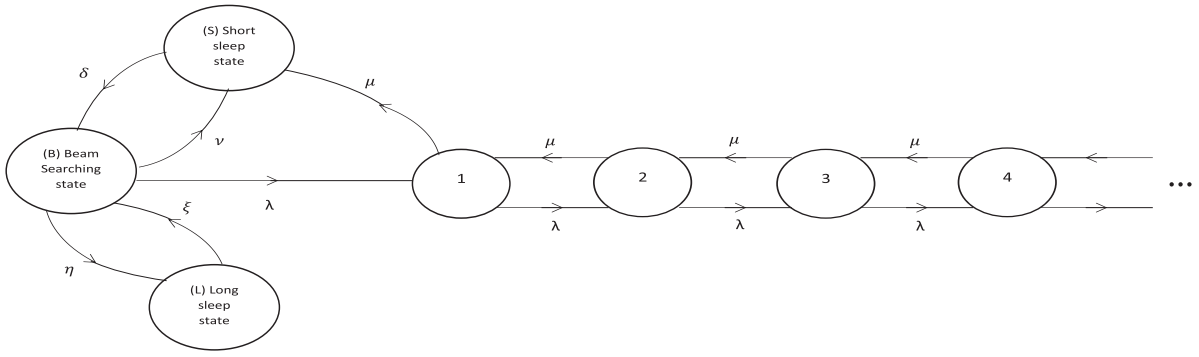

FIGURE 1. State transition diagram for Beam-Alignment DRX mechanism.

long-sleep period depending upon the availability of new downlink data packets. The state transition diagram for the 5G-DRX beamforming queuing system under investigation is displayed in Figure 1.

3. Transient probability distribution

We can model the proposed 5G-DRX beamforming mechanism using a continuous time Markov chain. Let $\{X(t) : t \in \mathbb{R}^+\}$ represent the state of the system at time t. Define $P_n(t) = P(X(t) = n)$ for $n = 1, 2, 3, \ldots$, as the transient probability of having "n" data packets in the system while the UE is in an active or busy state. Let $P_L(t) = P(X(t) = L)$ represent the probability that the UE is in long-sleep state, $P_S(t) = P(X(t) = S)$ denote the probability that the UE is in the short-sleep state, and $P_B(t) = P(X(t) = B)$ indicate the probability that the UE is in the beam alignment state at time t. Therefore, the state space of the UE is $\Omega = \{S, B, L, 1, 2, 3, \ldots, \}$.

By employing basic principles of probability, the transient probabilities $P_n(t) = P(X(t) = n)$, $n \in \Omega$ satisfy the following Kolmogorov forward equations:

$$\frac{\mathrm{d}P_L(t)}{\mathrm{d}t} = -\xi P_L(t) + \eta P_B(t), \tag{3.1}$$

$$\frac{\mathrm{d}P_B(t)}{\mathrm{d}t} = -(\lambda + \nu + \eta)P_B(t) + \delta P_S(t) + \xi P_L(t), \tag{3.2}$$

$$\frac{\mathrm{d}P_S(t)}{\mathrm{d}t} = -\delta P_S(t) + \mu P_1(t) + \nu P_B(t), \tag{3.3}$$

$$\frac{\mathrm{d}P_1(t)}{\mathrm{d}t} = -(\lambda + \mu)P_1(t) + \lambda P_B(t) + \mu P_2(t), \tag{3.4}$$

$$\frac{\mathrm{d}P_n(t)}{\mathrm{d}t} = -(\lambda + \mu)P_n(t) + \lambda P_{n-1}(t) + \mu P_{n+1}(t), \ n = 2, 3, 4, \ldots \ . \tag{3.5}$$

Assume, for simplicity, that at the initial time only one data packet is in the active state of the UE, *i.e.*,

$$P_1(0) = 1, \text{ and } P_n(0) = 0, \qquad n \neq 1. \tag{3.6}$$

In the subsequent analysis, let $f^*(s)$ represent the Laplace transform (LT) of the function $f(t)$. By applying LTs and rearranging the terms, the aforementioned equations lead to the following system of simultaneous equations:

$$(s + \xi)P_L^*(s) = \eta P_B^*(s), \tag{3.7}$$

$$(s + \lambda + \nu + \eta)P_B^*(s) = \delta P_S^*(s) + \xi P_L^*(s), \tag{3.8}$$

$$(s + \delta)P_S^*(s) = \mu P_1^*(s) + \nu P_B^*(s), \tag{3.9}$$

$$(s+\lambda+\mu)P_1^*(s) = 1 + \lambda P_B^*(s) + \mu P_2^*(s), \tag{3.10}$$

$$(s+\lambda+\mu)P_n^*(s) = \lambda P_{n-1}^*(s) + \mu P_{n+1}^*(s), \quad n = 2,3,4,\ldots \tag{3.11}$$

where we have utilized the initial conditions (3.6).

We now express (3.11) as the forward difference system of recurrence relations

$$\frac{P_n^*(s)}{P_{n-1}^*(s)} = \frac{\lambda}{(s+\lambda+\mu) - \mu\frac{P_{n+1}^*(s)}{P_n^*(s)}}, \quad n = 2,3,4,\ldots\ . \tag{3.12}$$

Through iterative operations, the above expressions transform into the form of a continued fraction

$$\frac{P_n^*(s)}{P_{n-1}^*(s)} = \frac{\lambda}{(s+\lambda+\mu) - \cfrac{\lambda\mu}{(s+\lambda+\mu) - \cfrac{\lambda\mu}{(s+\lambda+\mu) - \cfrac{\lambda\mu}{(s+\lambda+\mu)-\cdots}}}}. \tag{3.13}$$

We now write the above as

$$\frac{P_n^*(s)}{P_{n-1}^*(s)} = \frac{\lambda}{(s+\lambda+\mu) - \phi(s)}, \tag{3.14}$$

where

$$\phi(s) = \frac{\lambda\mu}{(s+\lambda+\mu) - \cfrac{\lambda\mu}{(s+\lambda+\mu) - \cfrac{\lambda\mu}{(s+\lambda+\mu) - \cfrac{\lambda\mu}{(s+\lambda+\mu)-\cdots}}}},$$

so that

$$\phi(s) = \frac{\lambda\mu}{(s+\lambda+\mu) - \phi(s)}. \tag{3.15}$$

It follows that $\phi(s)$ satisfies the quadratic equation:

$$\phi^2(s) - (s+\lambda+\mu)\phi(s) + \lambda\mu = 0. \tag{3.16}$$

For $s > 0$, there exist two positive solutions to (3.16) which are given by

$$\phi_+(s), \phi_-(s) = \frac{(s+\mu+\lambda) \pm \sqrt{(s+\lambda+\mu)^2 - 4\lambda\mu}}{2}. \tag{3.17}$$

Note that $\phi(\infty) = 0$ is a necessary condition for $\phi(s)$ to be the LT of the probability distribution function of a random variable (see [43]). Clearly, only $\phi_-(s)$ fulfills this required condition and it is the minimal positive unique solution of (3.16). Therefore, to proceed further we choose $\phi(s) = \phi_-(s)$.

Thus, substituting the expression of $\phi_-(s)$ for $\phi(s)$ into (3.14), we have

$$\frac{P_n^*(s)}{P_{n-1}^*(s)} = \frac{\lambda}{(s+\lambda+\mu) - \left[\frac{(s+\lambda+\mu) - \sqrt{(s+\lambda+\mu)^2 - 4\lambda\mu}}{2}\right]}, \quad n = 2,3,4,\ldots.$$

Algebraic simplification of the above yields

$$P_n^*(s) = \left[\frac{(s+\lambda+\mu) - \sqrt{(s+\lambda+\mu)^2 - \alpha^2}}{2\mu}\right] P_{n-1}^*(s), \quad n = 2,3,4,\ldots, \tag{3.18}$$

where $\alpha = 2\sqrt{\lambda\mu}$.

Iteration of (3.18) gives

$$P_n^*(s) = \left[\frac{(s+\lambda+\mu) - \sqrt{(s+\lambda+\mu)^2 - \alpha^2}}{2\mu}\right]^{n-1} P_1^*(s), \quad n = 2, 3, 4, \ldots. \tag{3.19}$$

In particular, for $n = 2$, the above expression becomes

$$P_2^*(s) = \left[\frac{(s+\lambda+\mu) - \sqrt{(s+\lambda+\mu)^2 - \alpha^2}}{2\mu}\right] P_1^*(s). \tag{3.20}$$

Next, by using (3.20) in (3.10) and performing some algebraic operations, it follows that

$$P_1^*(s) = \frac{1}{\left[\frac{(s+\lambda+\mu)+\sqrt{(s+\lambda+\mu)^2-\alpha^2}}{2}\right]} + \frac{\lambda P_B^*(s)}{\left[\frac{(s+\lambda+\mu)+\sqrt{(s+\lambda+\mu)^2-\alpha^2}}{2}\right]}$$

whence

$$P_1^*(s) = \frac{(s+\lambda+\mu) - \sqrt{(s+\lambda+\mu)^2 - \alpha^2}}{2\lambda\mu} + \frac{(s+\lambda+\mu) - \sqrt{(s+\lambda+\mu)^2 - \alpha^2}}{2\mu} P_B^*(s). \tag{3.21}$$

Now, from the linear equations (3.7), (3.8) and (3.9), respectively, we have

$$P_L^*(s) = \frac{\eta}{s+\xi} P_B^*(s), \tag{3.22}$$

$$P_B^*(s) = \frac{\delta}{(s+\lambda+\nu+\eta)} P_S^*(s) + \frac{\xi}{(s+\lambda+\nu+\eta)} P_L^*(s), \tag{3.23}$$

$$P_S^*(s) = \frac{\mu}{s+\delta} P_1^*(s) + \frac{\nu}{s+\delta} P_B^*(s). \tag{3.24}$$

Using (3.24) in (3.23) gives

$$(s+\lambda+\nu+\eta) P_B^*(s) = \delta\left[\frac{\mu}{(s+\delta)} P_1^*(s) + \frac{\nu}{(s+\delta)} P_B^*(s)\right] + \frac{\eta\xi}{(s+\xi)} P_B^*(s). \tag{3.25}$$

Next, plugging (3.21) into (3.25) and solving for $P_B^*(s)$, we arrive at

$$P_B^*(s) = \frac{\frac{\delta}{(s+\delta)}\left[\frac{(s+\lambda+\mu)-\sqrt{(s+\lambda+\mu)^2-\alpha^2}}{2\lambda}\right]}{\left\{(s+\lambda+\nu+\eta) - \frac{\nu\delta}{s+\delta} - \frac{\eta\xi}{s+\xi} - \frac{\delta}{s+\delta}\left[\frac{(s+\lambda+\mu)-\sqrt{(s+\lambda+\mu)^2-\alpha^2}}{2}\right]\right\}}. \tag{3.26}$$

In fact the above can be expressed, after straight forward calculus, as

$$P_B^*(s) = \frac{\frac{\delta}{(\lambda+\nu+\eta-\delta)}\left[\frac{1}{s+\delta} - \frac{1}{s+\lambda+\nu+\eta}\right]\left[\frac{(s+\lambda+\mu)-\sqrt{(s+\lambda+\mu)^2-\alpha^2}}{2\lambda}\right]}{1 - H^*(s)}, \tag{3.27}$$

in which

$$H^*(s) = \frac{\nu\delta}{(\lambda+\nu+\eta-\delta)}\left[\frac{1}{s+\delta} - \frac{1}{s+\lambda+\nu+\eta}\right] + \frac{\eta\xi}{(\lambda+\nu+\eta-\xi)}\left[\frac{1}{s+\xi} - \frac{1}{s+\lambda+\nu+\eta}\right]$$

$$+\frac{\delta}{(\lambda+\nu+\eta-\delta)}\left[\frac{1}{s+\delta}-\frac{1}{(s+\lambda+\nu+\eta)}\right]\left[\frac{(s+\lambda+\mu)-\sqrt{(s+\lambda+\mu)^2-\alpha^2}}{2}\right] \tag{3.28}$$

with $\lambda+\nu+\eta\neq\delta$ and $\lambda+\nu+\eta\neq\xi$. It can be seen that $|H^*(s)|<1$. The proof of this assertion is proved in Appendix A.

Thus, the expression for $P_B^*(s)$ may be readily obtained in the form

$$\begin{aligned}P_B^*(s)=\frac{\delta}{(\lambda+\nu+\eta-\delta)}&\left\{\frac{1}{(s+\delta)}\left[\frac{(s+\lambda+\mu)-\sqrt{(s+\lambda+\mu)^2-\alpha^2}}{2\lambda}\right]\right.\\&\left.-\frac{1}{(s+\lambda+\nu+\eta)}\left[\frac{(s+\lambda+\mu)-\sqrt{(s+\lambda+\mu)^2-\alpha^2}}{2\lambda}\right]\right\}\left[1+\sum_{n=1}^{\infty}(H^*(s))^n\right].\end{aligned} \tag{3.29}$$

Upon inversions, (3.29) and (3.28), respectively, yield

$$\begin{aligned}P_B(t)=\frac{\delta}{(\lambda+\nu+\eta-\delta)}&\left\{\int_0^t e^{-\delta(t-u)}\beta^{-1}e^{-(\lambda+\mu)u}\frac{I_1(\alpha u)}{u}\,\mathrm{d}u\right.\\&\left.-\int_0^t e^{-(\lambda+\nu+\eta)(t-u)}\beta^{-1}e^{-(\lambda+\mu)u}\frac{I_1(\alpha u)}{u}\,\mathrm{d}u\right\}\\&+\frac{\delta}{(\lambda+\nu+\eta-\delta)}\left\{\int_0^t e^{-\delta(t-u)}\int_0^u\beta^{-1}e^{-(\lambda+\mu)(u-v)}\frac{I_1(\alpha(u-v))}{(u-v)}\right.\\&\times\sum_{n=1}^{\infty}H^{©(n)}(v)\,\mathrm{d}v\,\mathrm{d}u-\int_0^t e^{-(\lambda+\nu+\eta)(t-u)}\int_0^u\beta^{-1}e^{-(\lambda+\mu)(u-v)}\\&\left.\times\frac{I_1(\alpha(u-v))}{(u-v)}\sum_{n=0}^{\infty}H^{©(n)}(v)\,\mathrm{d}v\,\mathrm{d}u\right\}\end{aligned} \tag{3.30}$$

and

$$\begin{aligned}H(t)=\frac{\nu\delta}{(\lambda+\nu+\eta-\delta)}&\left[e^{-\delta t}-e^{-(\lambda+\eta+\nu)t}\right]+\frac{\eta\xi}{(\lambda+\nu+\eta-\xi)}\left[e^{-\xi t}-e^{-(\lambda+\nu+\eta)t}\right]\\&+\frac{\delta}{(\lambda+\nu+\eta-\delta)}\left[\lambda\int_0^t e^{-\delta(t-u)}\beta^{-1}e^{-(\lambda+\mu)u}\frac{I_1(\alpha u)}{u}\,\mathrm{d}u\right.\\&\left.-\lambda\int_0^t e^{-(\lambda+\nu+\eta)(t-u)}\beta^{-1}e^{-(\lambda+\mu)u}\frac{I_1(\alpha u)}{u}\,\mathrm{d}u\right]\end{aligned} \tag{3.31}$$

in which $\beta=\sqrt{\frac{\lambda}{\mu}}$ and $H^{©(n)}(t)$ represents the *n-fold* convolution of $H(t)$ with itself. On account of (3.19), (3.21) and (3.24), we have

$$\begin{aligned}P_S^*(s)=\frac{\mu}{(s+\delta)}&\left\{\frac{1}{\lambda}\left[\frac{(s+\lambda+\mu)-\sqrt{(s+\lambda+\mu)^2-\alpha^2}}{2\mu}\right]\right.\\&\left.+\left[\frac{(s+\lambda+\mu)-\sqrt{(s+\lambda+\mu)^2-\alpha^2}}{2\mu}\right]P_B^*(s)\right\}+\frac{\nu}{s+\delta}\,P_B^*(s)\end{aligned} \tag{3.32}$$

and for $n=1,2,3,\ldots,$

$$P_n^*(s)=\frac{1}{\lambda}\left[\frac{(s+\lambda+\mu)-\sqrt{(s+\lambda+\mu)^2-\alpha^2}}{2\mu}\right]^n$$

$$+\left[\frac{(s+\lambda+\mu)-\sqrt{(s+\lambda+\mu)^2-\alpha^2}}{2\mu}\right]^n P_B^*(s). \tag{3.33}$$

On inversions of (3.22), (3.32) and (3.33), respectively, yield

$$P_L(t)=\int_0^t P_B(u)\,\eta\,e^{-\xi(t-u)}\,\mathrm{d}u, \tag{3.34}$$

$$\begin{aligned}P_S(t)&=\int_0^t \beta^{-1}e^{-(\lambda+\mu)u}\frac{I_1(u)}{u}e^{-\delta(t-u)}\,\mathrm{d}u\\&\quad+\int_0^t P_B(t-u)\lambda\int_0^u \beta^{-1}e^{-(\lambda+\mu)v}\,\frac{I_1(\alpha v)}{v}e^{-\delta(u-v)}\,\mathrm{d}v\,\mathrm{d}u+\int_0^t P_B(u)\nu e^{-\delta(t-u)}\,\mathrm{d}u,\end{aligned} \tag{3.35}$$

and for $n=1,2,3,\ldots,$

$$P_n(t)=\frac{1}{\lambda}\,n\,\beta^n e^{-(\lambda+\mu)t}\frac{I_n(\alpha t)}{t}+\int_0^t P_B(u)\,n\,\beta^n e^{-(\lambda+\mu)(t-u)}\frac{I_n(\alpha(t-u))}{(t-u)}\,\mathrm{d}u, \tag{3.36}$$

where the probability $P_B(u)$ is given in (3.30).

Therefore, the explicit analytical expressions for the transient probabilities of the system being studied are given in (3.34)–(3.36) and (3.30).

4. Virtual delay time

This section aims to assess the time-dependent performance metrics of the proposed 5G-DRX energy management system. Specifically, it will calculate the complementary cumulative distributive function of $X(t)$ and the expected virtual delay time $\mathrm{E}(W(t))$ at time t for the proposed 5G-DRX energy management wireless system. The virtual delay time at a particular instant is defined as the time until the UE is ready to transmit a virtual data packet that arrives exactly at that time instant.

The complementary cumulative distribution function of the number of data packets, $X(t)$, in the 5G-DRX system at time t is given by:

$$\begin{aligned}P(X(t)\geq k)=\sum_{n=k}^{\infty}P_n(t)&=\frac{1}{\lambda}\sum_{n=k}^{\infty}n\beta^n\frac{I_n(\alpha t)}{t}e^{-(\lambda+\mu)t}\\&\quad+\int_0^t\sum_{n=k}^{\infty}n\beta^n\frac{I_n(\alpha(t-u))}{(t-u)}e^{-(\lambda+\mu)(t-u)}P_B(u)\,\mathrm{d}u.\end{aligned} \tag{4.1}$$

The mean of $X(t)$, denoted as $m(t)=\mathrm{E}(X(t))$, is expressed as

$$\begin{aligned}m(t)=\sum_{k=1}^{\infty}P(X(t)\geq k)&=\frac{1}{\lambda}\sum_{k=1}^{\infty}\sum_{n=k}^{\infty}n\beta^n\frac{I_n(\alpha t)}{t}e^{-(\lambda+\mu)t}\\&\quad+\int_0^t\sum_{k=1}^{\infty}\sum_{n=k}^{\infty}n\beta^n\frac{I_n(\alpha(t-u))}{(t-u)}e^{-(\lambda+\mu)(t-u)}P_B(u)\,\mathrm{d}u,\end{aligned}$$

which leads to

$$\begin{aligned}m(t)&=\frac{1}{\lambda}\sum_{n=1}^{\infty}n^2\beta^n\frac{I_n(\alpha t)}{t}e^{-(\lambda+\mu)t}\\&\quad+\int_0^t\sum_{n=1}^{\infty}n^2\beta^n\frac{I_n(\alpha(t-u))}{(t-u)}e^{-(\lambda+\mu)(t-u)}P_B(u)\,\mathrm{d}u.\end{aligned} \tag{4.2}$$

Next, we establish the relationship between virtual delay time, $W(t)$, and the number of data packets, $X(t)$, in the proposed scheme at time t. This relationship is expressed as $W(t) = \sum_{i=1}^{X(t)} Y_i$, where Y_i represents the exponential service times of the data packets with rate μ. As a result, the expected virtual delay time $\mathrm{E}(W(t))$ for the data packets in the 5G-DRX mechanism at t is calculated as follows:

$$\mathrm{E}(W(t)) = \mathrm{E}(X(t))\mathrm{E}(Y_i) = \frac{1}{\mu}\, m(t).$$

Finally, by virtue of (4.2), the above becomes

$$\begin{aligned}\mathrm{E}(W(t)) = {} & \frac{2}{\alpha\mu}\sum_{n=1}^{\infty} n^2\beta^{n-1}\frac{I_n(\alpha t)}{t}e^{-(\lambda+\mu)t} \\ & + \frac{1}{\mu}\int_0^t \sum_{n=1}^{\infty} n^2\beta^n \frac{I_n(\alpha(t-u))}{(t-u)}e^{-(\lambda+\mu)(t-u)}P_B(u)\,\mathrm{d}u. \end{aligned} \tag{4.3}$$

5. First-passage time to long-sleep period

First-passage time (FPT) problems are a central feature of many practical applications, such as reliability analysis of computer networks, performance evolution of telecommunication systems, and the determination of the first battery life time outage probabilities of user equipments in a finite time horizon. Additionally, they pertain to scenarios where, at the first instance, the user's equipment switches to sleep states when there are no packets to transmit during the 5G-DRX beam search process.

In the proposed 5G-DRX scheme, a known fact is that the longer period of sleeping reduces the energy consumption and network cost but increases the mean delay time. Thus, it is necessary to explore the trade-off between the power saving and the delay time. To accomplish this, we examine here the structural properties of the FPT to the long-sleep states of the UE and the mean delay time of data packets during this period. This analysis helps in understanding how adjustments in sleeping duration impact both energy efficiency and data packet latency in the system.

5.1. Time to enter the long-sleep state

Let T be the random variable representing the duration of the FPT to reach the long-sleep state L, and let $f_L(t)$ represents its probability density function (p.d.f). In order to analyze the FPT to the state L, we set $\xi = 0$ and recall that $P_1(0) = 1$, so that (3.1), (3.29) and (3.28) are transformed into

$$f_L(t) \equiv \frac{\mathrm{d}P_L(t)}{\mathrm{d}t} = \eta P_B(t), \tag{5.1}$$

$$\begin{aligned} P_B^*(s) = {} & \frac{\delta}{(\lambda+\nu+\eta-\delta)}\left\{\frac{1}{(s+\delta)}\left[\frac{(s+\lambda+\mu)-\sqrt{(s+\lambda+\mu)-\alpha^2}}{2\lambda}\right]\right. \\ & \left. - \frac{1}{(s+\lambda+\nu+\eta)}\left[\frac{(s+\lambda+\mu)-\sqrt{(s+\lambda+\mu)-\alpha^2}}{2\lambda}\right]\right\}\left[1+\sum_{n=1}^{\infty}(H^*(s))^n\right] \end{aligned} \tag{5.2}$$

with

$$\begin{aligned} H^*(s) = {} & \frac{\delta}{(\lambda+\nu+\eta-\delta)}\left\{\frac{1}{(s+\delta)}\left[\frac{(s+\lambda+\mu)-\sqrt{(s+\lambda+\mu)^2-\alpha^2}}{2}\right]\right. \\ & \left. - \frac{1}{(s+\lambda+\nu+\eta)}\left[\frac{(s+\lambda+\mu)-\sqrt{(s+\lambda+\mu)^2-\alpha^2}}{2}\right]\right\} \end{aligned}$$

$$+\frac{\nu\delta}{(\lambda+\nu+\eta-\delta)}\left[\frac{1}{(s+\delta)}-\frac{1}{(s+\lambda+\nu+\eta)}\right]. \tag{5.3}$$

Inverse transforms of (5.2) and (5.3), respectively, yield

$$\begin{aligned}P_B(t)=&\frac{\delta}{(\lambda+\eta+\nu-\delta)}\left\{\int_0^t e^{-\delta(t-u)}\beta^{-1}e^{-(\lambda+\mu)u}\frac{I_1(\alpha u)}{u}\,\mathrm{d}u\right.\\&\left.-\int_0^t e^{-(\lambda+\nu+\eta)(t-u)}\beta^{-1}e^{-(\lambda+\mu)u}\frac{I_1(\alpha u)}{u}\,\mathrm{d}u\right\}\\&+\frac{\delta}{(\lambda+\eta+\nu-\delta)}\left\{\int_0^t e^{-\delta(t-u)}\int_0^u \beta^{-1}e^{-(\lambda+\mu)(u-v)}\frac{I_1(\alpha(u-v))}{(u-v)}\sum_{n=1}^{\infty}H^{©(n)}(v)\,\mathrm{d}v\,\mathrm{d}u\right.\\&\left.-\int_0^t e^{-(\lambda+\nu+\eta)(t-u)}\int_0^u \beta^{-1}e^{-(\lambda+\mu)(u-v)}\frac{I_1(\alpha(u-v))}{(u-v)}\sum_{n=1}^{\infty}H^{©(n)}(v)\,\mathrm{d}v\,\mathrm{d}u\right\},\end{aligned} \tag{5.4}$$

and

$$\begin{aligned}H(t)=&\frac{\delta}{(\lambda+\eta+\nu-\delta)}\left\{\lambda\int_0^t e^{-\delta(t-u)}\beta^{-1}e^{-(\lambda+\mu)u}\frac{I_1(\alpha u)}{u}\,\mathrm{d}u\right.\\&\left.-\lambda\int_0^t e^{-(\lambda+\nu+\eta)(t-u)}\beta^{-1}e^{-(\lambda+\mu)u}\frac{I_1(\alpha u)}{u}\,\mathrm{d}u\right\}+\frac{\nu\delta}{(\lambda+\nu+\eta-\delta)}\left[e^{-\delta t}-e^{-(\lambda+\nu+\eta)t}\right].\end{aligned} \tag{5.5}$$

Finally, by combining (5.1) and the result from (5.4), we get an exact analytic expression for the p.d.f of the FPT to the long-sleep state L in our 5G-DRX energy saving scheme, given by

$$\begin{aligned}f_L(t)\equiv&\frac{\mathrm{d}P_L(t)}{\mathrm{d}t}\\=&\frac{\eta\delta}{(\lambda+\eta+\nu-\delta)}\left\{\int_0^t e^{-\delta(t-u)}\beta^{-1}e^{-(\lambda+\mu)u}\frac{I_1(\alpha u)}{u}\,\mathrm{d}u-\int_0^t e^{-(\lambda+\nu+\eta)(t-u)}\beta^{-1}e^{-(\lambda+\mu)u}\frac{I_1(\alpha u)}{u}\,\mathrm{d}u\right\}\\&+\frac{\eta\delta}{(\lambda+\eta+\nu-\delta)}\left\{\int_0^t e^{-\delta(t-u)}\int_0^u \beta^{-1}e^{-(\lambda+\mu)(u-v)}\frac{I_1(\alpha(u-v))}{(u-v)}\sum_{n=1}^{\infty}H^{©(n)}(v)\,\mathrm{d}v\,\mathrm{d}u\right.\\&\left.-\int_0^t e^{-(\lambda+\nu+\eta)(t-u)}\int_0^u \beta^{-1}e^{-(\lambda+\mu)(u-v)}\frac{I_1(\alpha(u-v))}{(u-v)}\sum_{n=1}^{\infty}H^{©(n)}(v)\,\mathrm{d}v\,\mathrm{d}u\right\}.\end{aligned} \tag{5.6}$$

It is noteworthy that the density function $f_L(t)$ is well-defined and non-defective only if $\lambda\le\mu$, because

$$P(T<\infty)=\int_0^{\infty}f_L(t)\,\mathrm{d}t\equiv f_L^*(0)=\begin{cases}1, & \text{if } \lambda\le\mu,\\ \frac{\frac{\mu}{\lambda}}{1+\frac{(\lambda-\mu)}{\eta}}, & \text{if } \lambda>\mu.\end{cases}$$

The result indicates that when $\lambda\le\mu$, the probability of reaching the long-sleep state L is one. However, if $\lambda>\mu$, there is a non-zero probability that the system fails to reach the long-sleep state L.

Next, by taking $\xi=0$ in (3.26) and performing straightforward calculations, we obtain

$$P_B^*(s)=\frac{\frac{\delta\left[(s+\lambda+\mu)-\sqrt{(s+\lambda+\mu)^2-4\lambda\mu}\right]}{2\lambda}}{\left\{(s+\delta)(s+\lambda+\eta+\delta)-\delta\left[\frac{(s+\lambda+\mu)-\sqrt{(s+\lambda+\mu)^2-4\lambda\mu}}{2}\right]-\nu\delta\right\}}.$$

Now differentiating the above resulting expression with respect to s and evaluating at $s = 0$, we have

$$\left.\frac{\mathrm{d}P_B^*(s)}{\mathrm{d}s}\right|_{s=0} = (-1)\frac{\left\{\left[\lambda+\nu+\eta+\frac{\mu\delta}{\mu-\lambda}\right]+\frac{\eta\delta}{\mu-\lambda}\right\}}{\eta^2\delta}.$$

Thus, we determine the expected value, $\mathrm{E}(T)$, of the FPT random variable T to reach the long-sleep state L as

$$\begin{aligned}\mathrm{E}(T) &= \int_0^\infty t f_L(t)\,\mathrm{d}t = \left\{(-1)\eta\frac{\mathrm{d}P_B^*(s)}{\mathrm{d}s}\right\}\Big|_{s=0} \\ &= \begin{cases}\frac{1}{\eta}\left[\frac{\lambda+\eta+\nu}{\delta}+\frac{\mu+\eta}{(\mu-\lambda)}\right], & \text{if } \lambda<\mu,\\ \infty, & \text{if } \lambda\geq\mu.\end{cases}\end{aligned} \tag{5.7}$$

5.2. Mean delay time during the first-passage time

In this subsection, we analyze the transient behaviour of the mean delay time $\mathrm{E}(W_L(t))$ at time t during the FPT. Let $m_L(t)$ represent the expected number of data packets at time t in the 5G-DRX beam forming system during the FPT to the long-sleep state L. Therefore, the FPT duration T starts with a data packet arrival at time $t = 0$.

For $\xi = 0$ and $t > 0$, we then have from (4.2) and (3.36),

$$\begin{aligned}m_L(t) \equiv \mathrm{E}(X_L(t)) &= \frac{1}{\lambda}\sum_{n=0}^{\infty} n^2\beta^n e^{-(\lambda+\mu)t}\frac{I_n(\alpha t)}{t} \\ &\quad + \int_0^t \sum_{n=1}^{\infty} n^2\beta^n \frac{I_n(\alpha(t-u))}{(t-u)} e^{-(\lambda+\mu)(t-u)} P_B(u)\,\mathrm{d}u,\end{aligned}$$

and

$$\begin{aligned}\sum_{n=1}^{\infty} P_n(t) &= \frac{1}{\lambda}\sum_{n=1}^{\infty} n\beta^n e^{-(\lambda+\mu)t}\frac{I_n(\alpha t)}{t} \\ &\quad + \int_0^t \sum_{n=1}^{\infty} n\beta^n e^{-(\lambda+\mu)(t-u)}\frac{I_n(\alpha(t-u))}{(t-u)} P_B(u)\,\mathrm{d}u,\end{aligned} \tag{5.8}$$

where $P_B(t)$ is given in (5.4). It is observed that the data packets can only be transmitted, if they arrive during the FPT and the system is in an active state at time t. Therefore, the transient average delay time $\mathrm{E}(W_L(t))$ must be normalized. Since each packet transmission requires an exponentially distributed time with the mean of $\frac{1}{\mu}$, we have for $t > 0$,

$$\mathrm{E}(\mathrm{W_L(t)}) = \frac{m_L(t)}{\mu[1-P_S(t)-P_L(t)-P_B(t)]} = \frac{m_L(t)}{\mu\sum_{n=1}^{\infty} P_n(t)},$$

so that

$$\mathrm{E}(W_L(t)) = \frac{\frac{2}{\alpha}\sum_{n=1}^{\infty} n^2\beta^{n-1}e^{-(\lambda+\mu)t}\frac{I_n(\alpha t)}{t} + \int_0^t \sum_{n=1}^{\infty} n^2\beta^n \frac{I_n(\alpha(t-u))}{(t-u)} P_B(u)\,\mathrm{d}u}{\mu\left[\frac{1}{\lambda}\sum_{n=1}^{\infty} n\beta^n e^{-(\mu+\lambda)t}\frac{I_n(\alpha t)}{t} + \int_0^t \sum_{n=1}^{\infty} n\beta^n e^{-(\lambda+\mu)(t-u)}\frac{I_n(\alpha(t-u))}{(t-u)} P_B(u)\,\mathrm{d}u\right]}, \tag{5.9}$$

where the expressions for $P_B(t)$ and $H(t)$ are provided in (5.4) and (5.5), respectively.

Remark 1. It is evident that $\mathrm{E}(W_L(t))$ represents the conditional average latency, considering only for the data packets transmitted by the UE.

Remark 2. For $\xi = 0$, it is clear that $[1 - P_S(t) - P_L(t) - P_B(t)]$ represents the probability that the UE is in an active state at time t and acts as the normalization constant.

6. Steady-state probability distribution

In this section, we will explore the structure of the steady-state distribution for the dynamic LTE DRX scheme under discussion, specifically focusing on the 5G-DRX beam tracking wireless system. From a practical perspective, the steady-state (*i.e.*, long-run or persistent) results are typically more useful than transient (*i.e.*, real-time) state probabilities, as the system may not offer manageable solutions for transient analysis. In fact, steady-state performance measures often serve as effective approximations for the transient behaviour even when time t is relatively moderate. Thus, long-run state probabilities offer valuable insights into transient state probabilities. Moreover, the long-run probabilities expose some interesting characteristics of real-life systems' design and operation.

For this purpose, assuming that $\lambda > 0$, $\mu > 0$, $\xi > 0$, $\eta > 0$, $\delta > 0$ and $\nu > 0$, we obtain from (3.26), after simple algebra, as

$$P_B^*(s) = \frac{\frac{\delta}{s+\delta}\left[\frac{(s+\lambda+\mu)-\sqrt{(s+\lambda+\mu)^2-\alpha^2}}{2\lambda}\right]}{\left\{(s+\lambda)+\frac{\nu s}{s+\delta}+\frac{\eta s}{s+\xi}-\frac{\delta}{s+\delta}\left[\frac{(s+\lambda+\mu)-\sqrt{(s+\lambda+\mu)^2-\alpha^2}}{2}\right]\right\}}. \tag{6.1}$$

To obtain the steady-state results, we assume that $\lambda < \mu$. Under this condition, expanding both the numerator and denominator in powers of s and simplifying algebraically, (6.1) results in

$$P_B^*(s) = \frac{\frac{\delta}{s+\delta}\left\{1-\frac{s}{\mu-\lambda}-\frac{s^2}{4\lambda(\mu-\lambda)}+\frac{1}{4\lambda}\frac{(\lambda+\mu)^2}{(\mu-\lambda)^3}s^2+o(s^3)\right\}}{s+\lambda+\frac{s\nu}{s+\delta}+\frac{s\eta}{s+\xi}-\frac{\delta}{s+\delta}\left\{\lambda-\frac{\lambda s}{\mu-\lambda}-\frac{s^2}{4(\mu-\lambda)}+\frac{1}{4}\frac{(\lambda+\mu)^2}{(\mu-\lambda)^3}s^2+o(s^3)\right\}}$$

whence, as $s \to 0$,

$$P_B^*(s) \sim \frac{\frac{\delta}{s+\delta}\left\{1-\frac{s}{(\mu-\lambda)}+o(s^2)\right\}}{s\left\{\frac{\nu}{s+\delta}+\frac{\eta}{s+\xi}+\frac{1}{s+\delta}\left[s+\lambda+\delta+\frac{\lambda\delta}{\mu-\lambda}+o(s)\right]\right\}}. \tag{6.2}$$

By invoking the Tauberian theorem, this results in

$$P_B = \lim_{s\to 0} sP_B^*(s) = \frac{\frac{1}{\lambda}}{\frac{\nu}{\lambda\delta}+\frac{1}{\delta}+\frac{\eta}{\lambda\xi}+\frac{1}{\lambda}+\frac{1}{\mu-\lambda}}. \tag{6.3}$$

Now from (3.21) and (3.22), by virtue of the Tauberian theorem, we arrive at, respectively,

$$P_1 = \lim_{s\to 0} sP_1^*(s) = \frac{\lambda}{\mu}P_B, \tag{6.4}$$

and

$$P_L = \lim_{s\to 0} sP_L^*(s) = \lim_{s\to 0}\frac{\eta}{s+\xi}(sP_B^*(s)) = \frac{\eta}{\xi}P_B.$$

By usage of (6.3), the above gives

$$P_L = \frac{\frac{\eta}{\lambda\xi}}{\left[\frac{\nu}{\lambda\delta}+\frac{1}{\delta}+\frac{\eta}{\lambda\xi}+\frac{1}{\lambda}+\frac{1}{\mu-\lambda}\right]}. \tag{6.5}$$

Again, usage of the Tauberian theorem, we obtain from (3.24) and (6.4) as

$$P_S = \lim_{s\to 0} sP_S^*(s) = \lim_{s\to 0}\frac{\mu}{s+\delta}sP_1^*(s) + \lim_{s\to 0}\frac{\nu}{s+\delta}sP_B^*(s)$$

$$= \frac{\mu}{\delta}P_1 + \frac{\nu}{\delta}P_B = \frac{\mu\lambda}{\mu\delta}P_B + \frac{\nu}{\delta}P_B.$$

Making use of (6.3) into the above expression results in

$$P_S = \frac{\left(\frac{1}{\delta} + \frac{\nu}{\lambda\delta}\right)}{\left[\frac{\nu}{\lambda\delta} + \frac{1}{\delta} + \frac{\eta}{\lambda\xi} + \frac{1}{\lambda} + \frac{1}{\mu-\lambda}\right]}. \tag{6.6}$$

Finally, applying the Tauberian theorem to (3.19) yields

$$P_n = \lim_{s\to 0} sP_n^*(s) = \lim_{s\to 0}\left\{\left[\frac{(s+\lambda+\mu) - \sqrt{(s+\lambda+\mu)^2 - \alpha^2}}{2\mu}\right] sP_1^*(s)\right\}, \quad n = 1, 2, 3, \ldots .$$

Thus,

$$P_n = \left(\frac{\lambda}{\mu}\right)^{n-1} P_1 = \left(\frac{\lambda}{\mu}\right)^n P_B, \quad n = 1, 2, 3, \ldots , \tag{6.7}$$

where (6.4) has been applied.

Now combining (6.3) and (6.7), we obtain the following:

$$P_n = \frac{\frac{1}{\lambda}\left(\frac{\lambda}{\mu}\right)^n}{\left[\frac{\nu}{\lambda\delta} + \frac{1}{\delta} + \frac{\eta}{\lambda\xi} + \frac{1}{\lambda} + \frac{1}{\mu-\lambda}\right]}, \; n = 1, 2, 3, \ldots . \tag{6.8}$$

Hence, (6.3), (6.5), (6.6) and (6.8) fully determine, the steady-state probabilities of the beamforming state P_B, the long-sleep state P_L, the short-sleep state P_S, and the probability P_n of "n" packets occupying the active state, where $n = 1, 2, 3, \ldots$, for the proposed LTE DRX mechanism in 5G wireless network.

7. Stationary performance characteristics

In this section, we present a few key performance metrics for the LTE DRX scheme in the 5G wireless data packet communication system under the ergodic condition $\rho = \frac{\lambda}{\mu} < 1$.

(1) The mean number, $\mathrm{E}(X)$, of data packets in the system is given by

$$\mathrm{E}(X) = \sum_{n=1}^{\infty} nP_n = \frac{\rho}{(1-\rho)^2} P_B \tag{7.1}$$

where the probability P_B is given in (6.3).

(2) The system throughput, U, of the proposed scheme is computed as

$$U = \mu \sum_{n=1}^{\infty} P_n = \frac{\lambda}{1-\rho} P_B. \tag{7.2}$$

(3) The effective arrival rate, λ_{eff}, which denotes the total arrival rate of the data packets when the system is in beamforming and active states as

$$\lambda_{\text{eff}} = \lambda\left[P_B + \sum_{n=1}^{\infty} P_n\right] = \frac{\lambda P_B}{1-\rho}. \tag{7.3}$$

Note that in the LTE DRX scheme, the effective arrival rate, λ_{eff}, of the data packets is equal to the system throughput, U, *i.e.*, $\lambda_{\text{eff}} = U$, which confirms the classical Burke's theorem [7] for the proposed 5G-DRX mechanism.

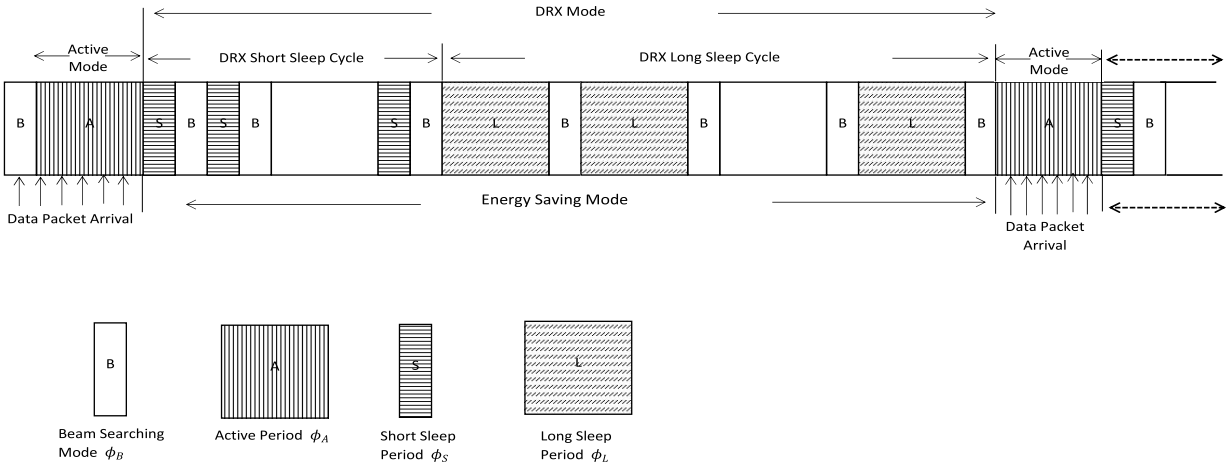

FIGURE 2. DRX operation of UE in 5G with Beam-Search state.

(4) The mean delay or sojourn time, $\mathrm{E}(W_S)$, of a data packet in 5G-DRX system is calculated using Little's law as

$$\mathrm{E}(W_S) = \frac{\mathrm{E}(X)}{\lambda_{\mathrm{eff}}} = \frac{1}{\mu - \lambda}. \tag{7.4}$$

(5) Recall that the regenerative cycle length, ϕ_{cycle}, for the proposed in 5G-DRX wireless system is the time elapsed between two consecutive data packet arrivals that finds the system empty (see [57]). Figure 2 illustrates a typical operation of the UE for the proposed LTE DRX in the 5G wireless integrating the beam searching state. In this figure, LTE DRX states are represented by rectangles labeled with letters "A", "S", "L", and "B" which correspond to the active, short-sleep, long-sleep and beamforming states of the UE, respectively. It is also observed from the figure that the cycle length ϕ_{cycle} includes the active period (ϕ_A), the short-sleep period (ϕ_S), the long-sleep period (ϕ_L) and the beamforming period (ϕ_B), of the UE. That is,

$$\phi_{\mathrm{cycle}} = \phi_S + \phi_L + \phi_A + \phi_B.$$

Moreover, since the underlying 5G-DRX wireless beam tracking system is a Markov process,

$$\mathrm{E}(\phi_S) = \frac{1}{\delta} + \frac{\nu}{\lambda\delta}, \quad \mathrm{E}(\phi_L) = \frac{\eta}{\xi}, \quad \mathrm{E}(\phi_A) = \frac{1}{\mu - \lambda} \text{ and } E(\phi_B) = \frac{1}{\lambda}. \tag{7.5}$$

Therefore, the mean regenerative cyclic time, $\mathrm{E}(\phi_{\mathrm{cycle}})$, for the 5G-DRX beam aligning system under discussion is given by

$$\begin{aligned} \mathrm{E}(\phi_{\mathrm{cycle}}) &= \mathrm{E}(\phi_S) + \mathrm{E}(\phi_L) + \mathrm{E}(\phi_A) + \mathrm{E}(\phi_B) \\ &= \frac{(\lambda + \nu)}{\lambda\delta} + \frac{\eta}{\xi} + \frac{1}{\mu - \lambda} + \frac{1}{\lambda}. \end{aligned} \tag{7.6}$$

(6) The expected number of unblocked data packets which are transmitted by the UE during the regenerative cycle is

$$\lambda_{\mathrm{eff}}\mathrm{E}(\phi_{\mathrm{cycle}}) = \frac{1}{1 - \rho}. \tag{7.7}$$

It is noteworthy that

$$\lambda_{\mathrm{eff}}\mathrm{E}(\phi_{\mathrm{cycle}}) = \mathrm{E}(\phi_A)\mu. \tag{7.8}$$

(7) The mean number, $\mathrm{E}(N_S)$, of unblocked data packets transmitted by the UE during the active period of the underlying 5G-DRX beamforming system is

$$\mathrm{E}(N_S) = \lambda[\mathrm{E}(\phi_B) + \mathrm{E}(\phi_A)] = \frac{1}{1-\rho}. \tag{7.9}$$

Finally, from the above results, one can establish a nice and vital relation, namely

$$\mathrm{E}(N_S) = \lambda_{\mathrm{eff}}\mathrm{E}(\phi_{\mathrm{cycle}}) = \mathrm{E}(\phi_A)\mu. \tag{7.10}$$

8. Average energy consumption and energy efficiency

In this part, we now focus on analyzing the energy efficiency and energy consumption factors of the UE.

The energy/power saving factor (ESF) is defined as the ratio of time the UE spends in the sleep states to the total time the UE spends in all the states. Hence,

$$\mathrm{ESF} = \frac{\frac{\nu}{\lambda\delta} + \frac{1}{\delta} + \frac{\eta}{\lambda\xi}}{\left[\frac{\nu}{\lambda\delta} + \frac{1}{\delta} + \frac{\eta}{\lambda\xi} + \frac{1}{\lambda} + \frac{1}{\mu-\lambda}\right]}. \tag{8.1}$$

The average energy consumption refers to the amount of energy used per data packet per unit of time by the UE utilizing the proposed 5G-DRX wireless system.

In other words, the average energy consumption is defined by long-run proportion of the total energy consumed by the UE over the entire time duration, *i.e.*,

$$\text{Average Energy Consumption} = \lim_{t\to\infty} \frac{\text{Energy consumed during } [0,t]}{t}.$$

According to the theory of renewal-reward processes [26], we have

$$P_{\mathrm{EC}} = \text{Average Energy Consumption} = \frac{\mathrm{E}(\text{Energy consumed during one cycle})}{\mathrm{E}(\phi_{\mathrm{cycle}})}, \tag{8.2}$$

where $\mathrm{E}(\phi_{\mathrm{cycle}})$ is defined in (7.6).

As a result,

$$P_{\mathrm{EC}} = \text{Average Energy Consumption} = \frac{\alpha_{\mathrm{SS}}\mathrm{E}(\phi_S) + \alpha_{LS}\mathrm{E}(\phi_L) + \alpha_{\mathrm{AP}}\mathrm{E}(\phi_A) + \alpha_{\mathrm{BIM}}\mathrm{E}(\phi_B)}{\mathrm{E}(\phi_S) + \mathrm{E}(\phi_L) + \mathrm{E}(\phi_A) + \mathrm{E}(\phi_B)}, \tag{8.3}$$

where $\alpha_{\mathrm{SS}}, \alpha_{\mathrm{LS}}, \alpha_{\mathrm{AP}}$ and α_{BIM} represent the energies consumed per unit of time of the UE in the short-sleep state, long-sleep state, active state and beamforming state, respectively.

By substituting (7.5) into (8.3), we have the average energy consumption per unit time of the UE in terms of the system parameters which is given by

$$P_{\mathrm{EC}} = \frac{\alpha_{\mathrm{SS}}\left(\frac{1}{\delta} + \frac{\nu}{\lambda\delta}\right) + \alpha_{\mathrm{SL}}\left(\frac{\eta}{\lambda\xi}\right) + \alpha_{\mathrm{AP}}\left(\frac{1}{\mu-\lambda}\right) + \alpha_{\mathrm{BIM}}\left(\frac{1}{\lambda}\right)}{\left(\frac{1}{\delta} + \frac{\nu}{\lambda\delta}\right) + \frac{\eta}{\lambda\xi} + \frac{1}{\mu-\lambda} + \frac{1}{\lambda}}. \tag{8.4}$$

To simultaneously evaluate two difference performance measures, namely system throughput U and average consumption per unit time P_{EC}, we introduce a new significance performance metric, termed energy efficiency, P_{EE} defined as the power/energy consumption per unit time per effective arrival for the proposed 5G-DRX scheme as

$$P_{\mathrm{EE}} = \frac{\mathrm{E}(\text{Total energy consumption})}{\mathrm{E}(\text{Throughput})} = \frac{P_{\mathrm{EC}}}{\mathrm{U}}. \tag{8.5}$$

Exploring (7.2) and (7.10) in the above leads to

$$P_{\mathrm{EE}} = \frac{P_{\mathrm{EC}}}{E(N_S)} = \left[\alpha_{\mathrm{SS}}\left(\frac{1}{\delta} + \frac{\nu}{\lambda\delta}\right) + \alpha_{\mathrm{SL}}\left(\frac{\eta}{\lambda\xi}\right) + \alpha_{\mathrm{AP}}\left(\frac{1}{\mu-\lambda}\right) + \alpha_{\mathrm{BIM}}\left(\frac{1}{\lambda}\right)\right](1-\rho). \tag{8.6}$$

Consecutively, P_{EE} is the average actual energy consumption to transmit a packet.

Remark 3. It is worth noting that the metrics "P_{EC}" and "P_{EE}" depend on the service time only through their means.

9. Time required to reach a specific critical number of packets in the base station buffer

Over the past decade, the FPT problem in queueing networks has been extensively studied due to its significance in both theoretical and applied contexts (see [22, 54]). We specifically aim to analyze the performance of FPT, which is not only important but also rarely investigated in wireless network communications. For instance, the FPT to reach a threshold level in the waiting line buffer at the eNB provides valuable insights for decision-making processes related to the design, control, efficient planning, and performance evaluation of wireless networks.

This section presents a study on the FPT to reach a specific threshold value/state, defined as $N \geq 1$ data packets, in the eNB's waiting line buffer of the 5G beam searching wireless communication system under the LTE DRX mechanism. The performance metrics of the FPT to reach the threshold value offer valuable insights into the behavior of the eNB's waiting line buffer and transmission channel, serving as an indicator of the system congestion. Frequent high buffer congestion can degrade data packet transmission quality, resulting in increased delays for data packets in the buffer. When this phenomenon occurs, the system administrator should take appropriate actions, such as regulating the processing of newly arrived packets, increasing the packet transmission rate, or extending the transmission channel's dwell time in the beamforming state. Therefore, the time required to reach a specific threshold level of the data packets in the waiting line buffer is a critical performance metric for the 5G-DRX beamforming wireless communication networks under discussion.

Related research on the FPT to reach a threshold level and its applications can be found in Chydzinski [9], Giorno and Nobile [15], Czachorski *et al.* [10], Krishna Kumar *et al.* [24, 25], and Park and Choi [40].

To analyse the FPT required to reach the predefined value/state N at the eNB's buffer, we utilize the convolution equations technique proposed by Choo and Conally [8]. This necessitates some definitions and notation. To this end, we define the random variable $T_n^{(N)}$ as the FPT to reach the predefined value N, starting from the previous state n, with the corresponding p.d.f denoted as $\phi_n(t)$, where $n \in \Omega_F = \{B, L, S, 1, 2, \ldots, N-1\}$. Figure 3 reveals the transition rate diagram for the FPT to reach the predefined value N which is an absorbing state for the system under study. So that, we have $\phi_N(t) = \delta(t)$ for the underlying 5G-DRX beamforming wireless radio network system, where $\delta(t)$ is the Dirac delta function.

Based on Figure 3, the following recursive convolution equations are obtained:

$$\begin{aligned}
\phi_S(t) &= \delta e^{-\delta t} \copyright \phi_B(t),\\
\phi_L(t) &= \xi e^{-\xi t} \copyright \phi_B(t),\\
\phi_B(t) &= \nu e^{-(\nu+\eta+\lambda)t} \copyright \phi_S((t) + \eta e^{-(\nu+\eta+\lambda)t} \copyright \phi L(t) + \lambda e^{-(\nu+\eta+\lambda)t}\phi_1(t),\\
\phi_1(t) &= \mu e^{-(\lambda+\mu)t} \copyright \phi_S(t) + \lambda e^{-(\lambda+\mu)t} \copyright \phi_2(t),\\
\phi_n(t) &= \mu e^{-(\lambda+\mu)t} \copyright \phi_{n-1}(t) + \lambda e^{-(\lambda+\mu)t} \copyright \phi_{n+1}(t), \quad n = 2, 3, \ldots, N-2,\\
\phi_{N-1}(t) &= \mu e^{-(\lambda+\mu)t} \copyright \phi_{N-2}(t) + \lambda e^{-(\lambda+\mu)t}.
\end{aligned} \tag{9.1}$$

where the symbol © represents the convolution operator. Unfortunately, we cannot determine an exact solution for the large value of N. Nevertheless, we have developed a method to compute the rth moment $M_n^{(N)}(r) =$

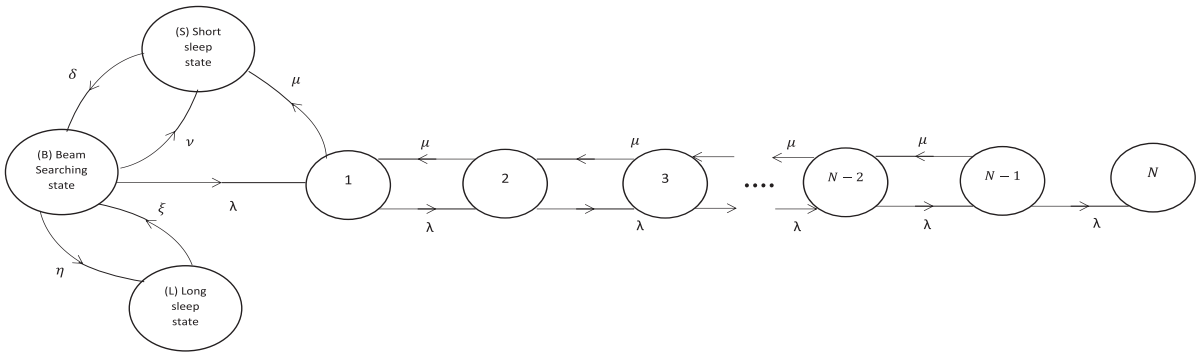

FIGURE 3. Flow diagram for Beam-Search DRX system with absorbing state N.

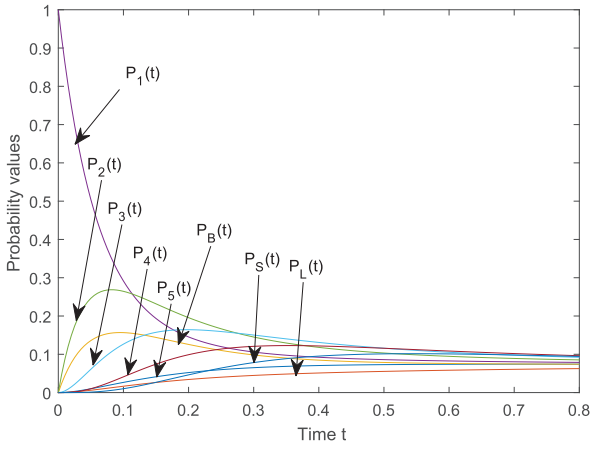

FIGURE 4. Probabilities $Pn(t)$ *versus* time t for $(\rho, \delta, \xi, \eta, \nu) = (0.5, 1.5, 1, 2, 2.5)$.

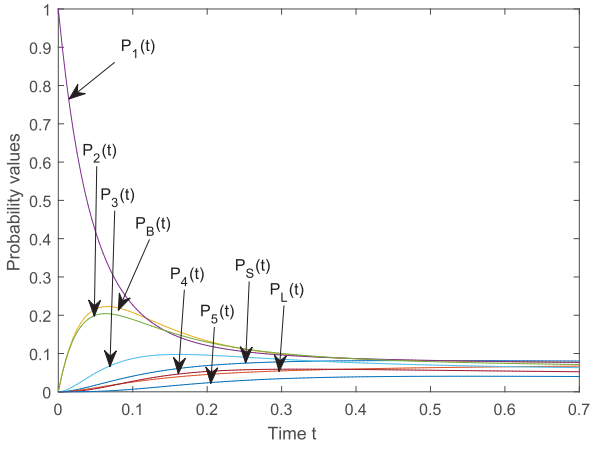

FIGURE 5. Probabilities $Pn(t)$ *versus* time t for $(\rho, \delta, \xi, \eta, \nu) = (1, 1.5, 1, 2, 2.5)$.

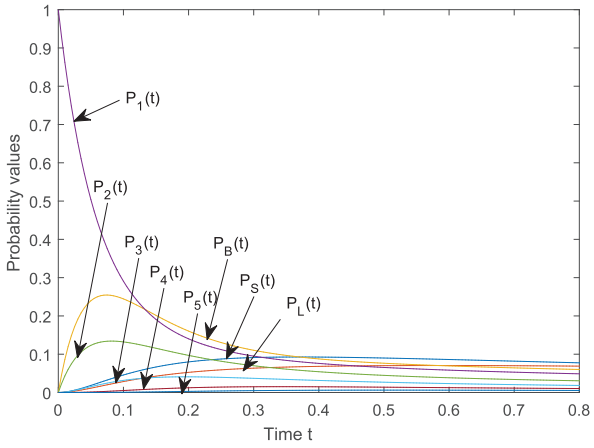

FIGURE 6. Probabilities $Pn(t)$ *versus* time t for $(\lambda, \mu, \delta, \xi, \eta, \nu) = (10, 5, 1.5, 1, 2, 2.5)$.

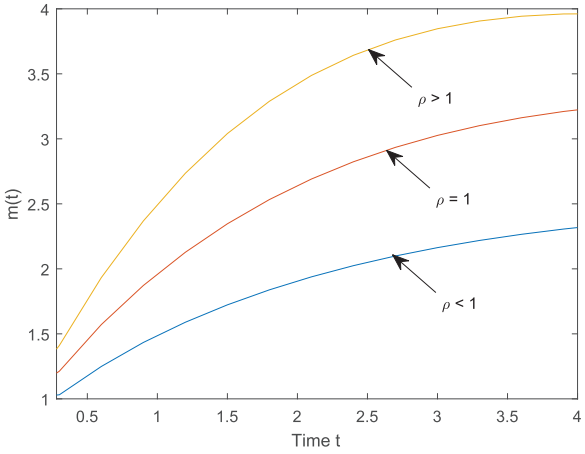

FIGURE 7. $m(t)$ *versus* time t for $(\delta, \xi, \eta, \nu) = (1.5, 1, 2, 2.5)$.

$\mathrm{E}((T_n^{(N)})^r)$ of $T_n^{(N)}$ for $r \geq 0$. To aid in this calculation, let $\phi_n^*(s)$ denote the LT of $\phi_n(t)$. Now, applying the LTs, doing some straightforward algebra, we obtain from (9.1) as:

$$\begin{aligned}
(s+\delta)\phi_S^*(s) - \delta\phi_B^*(s) &= 0,\\
(s+\xi)\phi_L^*(s) - \xi\phi_B^*(s) &= 0,\\
(s+\nu+\eta+\lambda)\phi_B^*(s) - \nu\phi_S^*(s) - \eta\phi_L^*(s) - \lambda\phi_1^*(s) &= 0,\\
(s+\lambda+\mu)\phi_1^*(s) - \mu\phi_S^*(s) - \lambda\phi_2^*(s) &= 0,\\
(s+\lambda+\mu)\phi_n^*(s) - \mu\phi_{n-1}^*(s) - \lambda\phi_{n+1}^*(s) &= 0, \quad n = 2, 3, \ldots, N-2,\\
(s+\lambda+\mu)\phi_{N-1}^*(s) - \mu\phi_{N-2}^*(s) &= \lambda.
\end{aligned} \tag{9.2}$$

The system of linear equations (9.2) can be rewritten in matrix form as:

$$\Delta_{(N+2)\times(N+2)}^{(N)}(s)\Phi_{(N+2)\times 1}^{(N)}(s) = \left[0, 0, 0, \ldots, \lambda\right]_{(N+2)\times 1}^{T}, \tag{9.3}$$

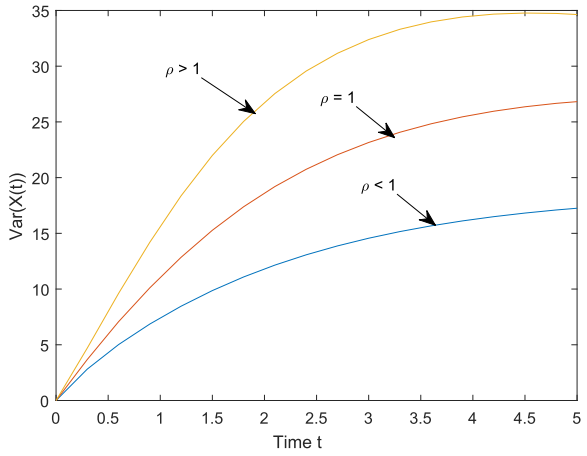

FIGURE 8. $Var(X(t))$ *versus* time t for $(\delta, \xi, \eta, \nu) = (1.5, 1, 2, 2.5)$.

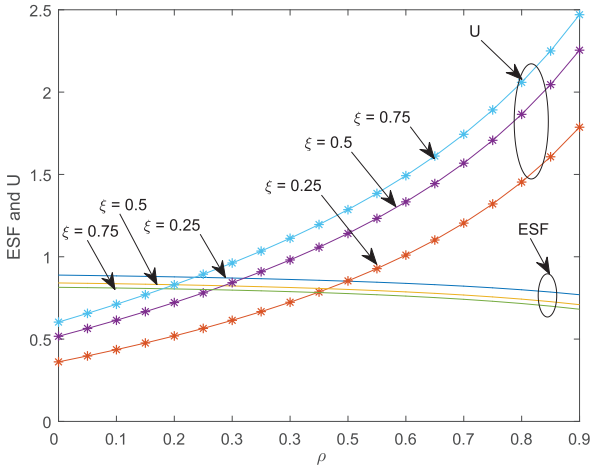

FIGURE 9. ESF and U *versus* ρ for $(\nu, \eta, \delta) = (2.5, 2, 1.5)$.

where

$$\Delta^{(N)}_{(N+2)\times(N+2)}(s) = sI_{N+2} - \Delta^{(N)}_{(N+2)\times(N+2)}$$

in which

$$\Delta^{(N)}_{(N+2)\times(N+2)} = \begin{bmatrix} -\delta & 0 & \delta & 0 & 0 & 0 \cdots 0 & 0 & 0 \\ 0 & -\xi & \xi & 0 & 0 & 0 \ldots 0 & 0 & 0 \\ \nu & \eta & -(\lambda+\nu+\eta) & \lambda & 0 & 0 \cdots 0 & 0 & 0 \\ \mu & 0 & 0 & -(\lambda+\mu) & \lambda & 0 \cdots 0 & 0 & 0 \\ 0 & 0 & 0 & \mu & -(\lambda+\mu) & \lambda \cdots 0 & 0 & 0 \\ \vdots & \vdots & \vdots & \vdots & \vdots & \vdots \ddots \vdots & \vdots & \vdots \\ 0 & 0 & 0 & 0 & 0 & 0 \; 0 \; \mu & -(\lambda+\mu) & \lambda \\ 0 & 0 & 0 & 0 & 0 & 0 \; 0 \; 0 & 0 & -\lambda \end{bmatrix}$$

$$\Phi^{(N)}_{(N+2)\times 1}(s) = \left[\Phi^*_S(s), \Phi^*_L(s), \Phi^*_B(s), \Phi^*_1(s), \ldots, \Phi^*_{N-2}(s), \Phi^*_{N-1}(s)\right]^T_{(N+2)\times 1},$$

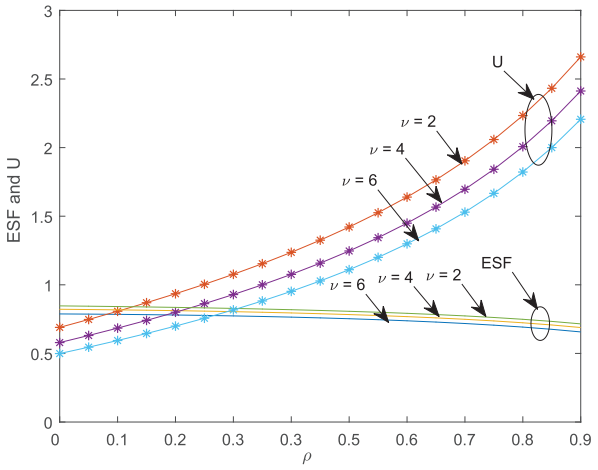

FIGURE 10. ESF and U *versus* ρ for $(\eta, \xi, \delta) = (2, 1, 1.5)$.

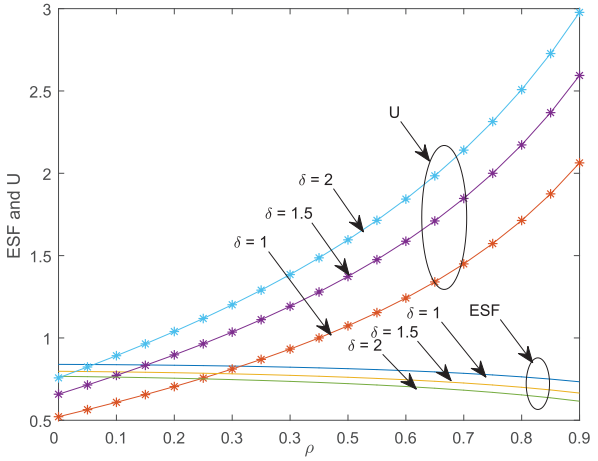

FIGURE 11. ESF and U *versus* ρ for $(\nu, \xi, \eta) = (2.5, 1, 2)$.

and I_{N+2} is the identity matrix of order $N+2$. To continue our discussion, we will organize the conditional moments $m_n^{(N)}(r)$, where $r \geq 0$, and $n \in \Omega_F$, according to the states as follows:

$$m^{(N)}(r) = \left[m_S^{(N)}(r), m_L^{(N)}(r), m_B^{(N)}(r), m_1^{(N)}(r), \ldots, m_{N-1}^{(N)}(r)\right]^T_{(N+2)\times 1} \quad \text{for } r \geq 0. \tag{9.4}$$

To obtain the conditional moments $m_n^{(N)}(r)$ for $r \geq 0$ recursively, we differentiate both sides of the equation (9.3) r-times with respect to s, and using the well known Leibniz's rule for derivatives:

$$\Delta^{(N)}_{(N+2)\times(N+2)}(s)\frac{d^r \Phi^{(N)}_{(N+2)\times(N+2)}(s)}{\mathrm{d}s^r} + r\frac{d^{r-1}\Phi^{(N)}_{(N+2)\times(N+2)}(s)}{\mathrm{d}s^{r-1}} = \mathbf{0}, \quad r \geq 1. \tag{9.5}$$

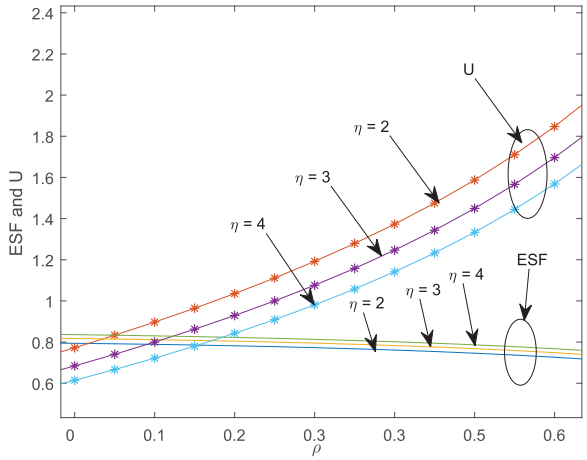

FIGURE 12. ESF and U *versus* ρ for $(\nu, \xi, \delta) = (2.5, 1, 1.5)$.

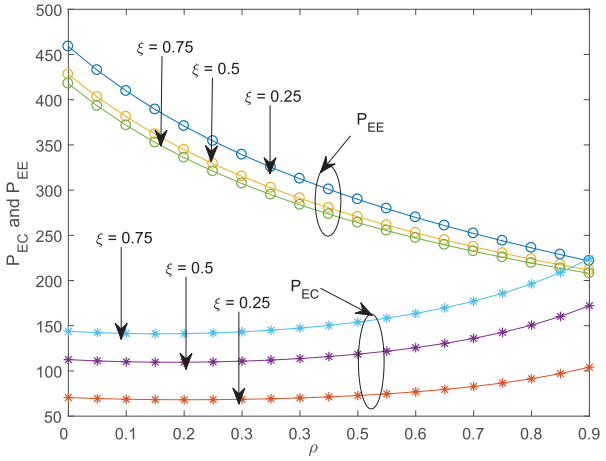

FIGURE 13. P_{EC} and P_{EE} *versus* ρ for $(\nu, \delta, \eta) = (2.5, 1.5, 2)$.

Noting that

$$m^{N}(r) = (-1)^{r} \frac{d^{r} \Phi^{(N)}_{(N+2)\times(N+2)}(s)}{\mathrm{d}s^{r}}\bigg|_{s=0} \quad \text{for } r \geq 1,$$

and $\Delta^{(N)}_{(N+2)\times(N+2)}(0) = \Delta^{(N)}_{(N+2)\times(N+2)}$, we can see that the vector of rth conditional moments (9.4) satisfies the following tridiagonal recurrence relation:

$$\Delta^{(N)}_{(N+2)\times(N+2)} m^{(N)}(r) = -r m^{(N)}(r-1), \quad r \geq 1,$$

with initial condition

$$m^{(N)}(0) = \big[1, 1, 1, \ldots, 1\big]^{T}_{(N+2)\times 1}. \tag{9.6}$$

Therefore, this set of equations enables us to compute the vector of rth conditional moments $m^{(N)}(r)$ for $r \geq 1$ in terms of the moments of the preceding order.

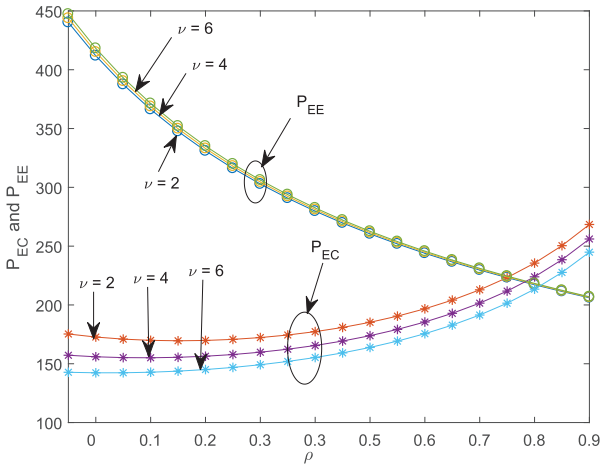

FIGURE 14. P_{EC} and P_{EE} *versus* ρ for $(\xi, \delta, \eta) = (2.5, 1.5, 2)$.

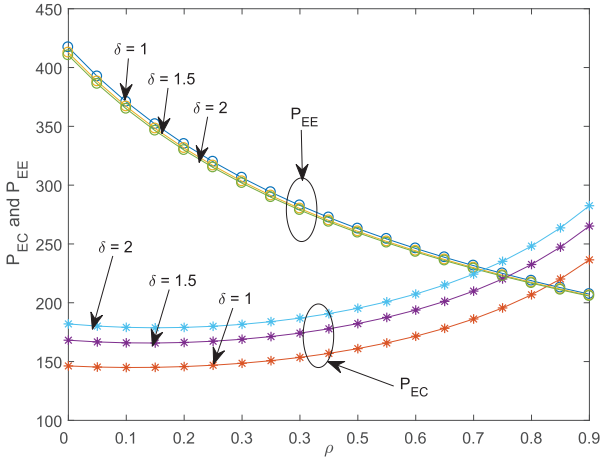

FIGURE 15. P_{EC} and P_{EE} *versus* ρ for $(\nu, \xi, \eta) = (2.5, 1, 2)$.

Specifically, by setting $r = 1$ and 2, we can determine the vectors representing the conditional mean $m^{(N)}(1)$ and second moment $m^{(N)}(2)$ of the FPT $T_n^{(N)}$ which reaches as predefined value/state, such as N number of data packets in the waiting line buffer, starting from any one of the previous state $n \in \Omega_F$ as

$$m_n^{(N)}(1) = -e_{N+2}(n)\left[\left(\Delta^{(N)}_{(N+2)\times(N+2)}\right)^{-1}[1, 1, 1, \ldots, 1]^T_{(N+2)\times 1}\right], \tag{9.7}$$

and

$$m_n^{(N)}(2) = e_{N+2}(n)\left[2\left(\Delta^{(N)}_{(N+2)\times(N+2)}\right)^{-2}[1, 1, 1, \ldots, 1]^T_{(N+2)\times 1}\right],$$

where $e_{N+2}(i)$ is a row vector of length $N+2$ whose entries are all zero, except for the ith entry, which is one.

Finally, the conditional variance $\mathrm{Var}(T_n^{(N)})$ of the FPT random variable $T_n^{(N)}$ is determined by

$$\mathrm{Var}(T_n^{(N)}) = m_n^{(N)}(2) - \left(m_n^{(N)}(1)\right)^2, \quad n \in \Omega_F.$$

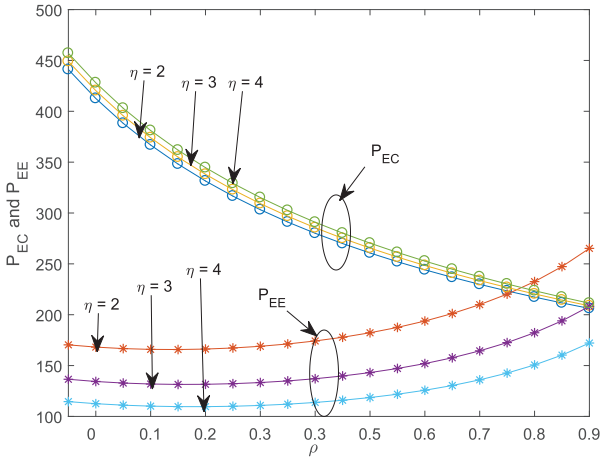

FIGURE 16. P_{EC} and P_{EE} *versus* ρ for $(\nu, \delta, \xi) = (2.5, 1.5, 2)$.

10. Numerical simulations and discussions

Our aim in this section is to provide the numerical results to evaluate the transient probabilities and time-dependent performance metrics for the proposed 5G-DRX beamforming scheme in certain typical system setups. The explicit analytical transient results have a complex structure, making their characteristics difficult to analyze directly. However, their dynamic behavior can be examined numerically by truncating the infinite-series convolution of functions in equation (3.28), as outlined in Appendix B, and then implementing the computational procedure using MATLAB V8.5 software With this objective, we examine how the system parameters influence the following descriptors as a function of time t:

(1) The transient state probabilities $P_B(t)$, $P_L(t)$, $P_S(t)$, and $P_n(t)$ for $n \geq 1$, of the UE over time t.
(2) The mean $m(t)$ and variance $Var(X(t))$ of the number of data packets in the system.

10.1. State probabilities *versus* time

First, we investigate the trend of probabilities $P_B(t)$, $P_L(t)$, $P_S(t)$, and $P_n(t)$ for $n \geq 1$, under three different traffic load settings $\rho = \frac{\lambda}{\mu}$: $\rho < 1$ (low), $\rho = 1$ (light), and $\rho > 1$ (heavy) in Figures 3–5. By choosing $(\delta, \xi, \eta, \nu) = (1.5, 1, 2, 2.5)$, it is evident from these figures that the curve of $P_1(t)$ starts at one initially and then decays exponentially, eventually reaching its steady-state value as time t progresses. Furthermore, the decay is faster and the steady-state is reached more quickly as time increases. In contrast, the probability curves for $P_B(t)$, $P_L(t)$, $P_S(t)$, and $P_n(t)$ where $n \geq 2$, start at the origin at $t = 0$, initially increasing to a certain extent, before gradually decreasing and approaching their equilibrium values as time t increases across all traffic load scenarios. Additionally, the curves of $P_B(t)$ remain at a higher level, while $P_L(t)$ stays at a lower level, with the curves of $P_S(t)$ positioned between $P_B(t)$ and $P_L(t)$ for all three traffic load cases. Finally, from these figures, we can infer that as the number of data packets n increases, the transient state probability curves exhibit a decreasing trend for a fixed value of t.

10.2. Trends of the time dependent performance indices

Here, Figure 6 reveals the characteristics of the mean $m(t)$ *versus* time t for three different traffic loads ρ. Evidently, the graph shows that initially all the curves rise up, but eventually they stabilize at their steady-state values. Additionally, the $m(t)$ curve for $\rho > 1$ consistently remains at the highest level compared to the curves for $\rho = 1$ and $\rho < 1$, as expected.

Next, we plot the variance $Var(X(t))$ as a function of time t for low ($\rho < 1$), light ($\rho = 1$) and heavy ($\rho > 1$) traffic loads in Figure 7. Examining the figure, it is evident that the trend is similar to that observed in Figure 6. However, the growth in $Var(X(t))$ is significantly more pronounced compared to the mean $m(t)$ over time t and it is eventually approaching a stationary value.

10.3. Trade-off analysis of energy efficiency and throughput

We now assess the performance of 5G-DRX for the beamforming scenario in a stationary regime. To achieve this, we study the impacts of the system parameters λ, μ, δ, ξ, η, and ν on the UE performance metrics. Of course, in all the numerical studies conducted below, we ensure that the parameter values meet the stability condition $\rho < 1$.

Figure 8 through Figure 11 elucidate the significant trade-offs between the energy-saving factor (ESF) and throughput (U) as the functions of the traffic load ρ. In Figure 8, we have plotted curves relating to ESF and U for different values of ξ when $(\nu, \eta, \delta) = (2.5, 2, 1.5)$. It is seen that as the traffic load ρ varies from 0 to 0.9, the ESF decays at a slower rate, whereas U rises rapidly which agrees with our intuition. Another observation from Figure 8 is that the ESF declines at a slower rate, while U rises significantly by increasing values of ξ for a fixed ρ. The reason for this is that as the mean time $\frac{1}{\xi}$ spending in the long-sleep (inactive) state decreases, the UE transits to the beamform state. Thus, the average energy consumption increases, and the transmission rate of the data packets also increases significantly.

In Figure 9, we change the values of ν and ρ and then plot the resulting values of ESF and U by taking $(\eta, \xi, \delta) = (2, 1, 1.5)$. As a result, Figure 9 exhibits similar characteristics to Figure 8, except that both the ESF and U decline with increasing values of ν for a fixed ρ. This phenomenon can be explained as follows: as the mean time spent in the beamforming state, $\frac{1}{\nu}$, decreases, the UE switches to the power saving short-sleep (inactive) state. Consequently, both the average energy consumption and the data packet transmission rate are reduced.

We now analyze the behaviors of ESF and U by varying the values of δ and ρ for the parameters $(\nu, \xi, \eta) = (2.5, 1, 2)$ in Figure 10. In this figure, it is shown that while the traffic load ρ increases, the throughput U of the system rises at the same time and the energy saving factor ESF declines significantly. Besides, with the larger value of δ, the throughput U is also high, whereas the energy saving factor (ESF) decreases for a given ρ. This scenario causes a smaller average dwelling time $\frac{1}{\delta}$ in the short-sleep state and hence the UE switches more frequently to the beamforming state, allowing more time to be allocated to beamforming. Hence, the average power consumption is increased relatively, whereas the transmission rate of the data packets is increased rapidly.

In Figure 11, the curves of ESF and U are plotted as functions of η and ρ, with parameters fixed at $(\nu, \xi, \delta) = (2.5, 1, 1.5)$. It can be observed that as ρ increases, U rises monotonically, whereas ESF declines at a slower rate for a given η, which aligns with our intuitive expectation. On the other hand, for any specific values of ρ, increasing η leads to a decrease in U, but a significant boost in ESF. This can be explained by the fact that as the mean residing time spent in the beamforming state, $\frac{1}{\eta}$, decreases, consequently the UE switches more frequently to the long-sleep state. Therefore, this results in a decline in data packet transmission, but an increase in the ESF.

10.4. Trade-off between energy efficiency and energy usage

In the following illustrations, we analyze how sensitive the average energy consumption (P_{EC}) and the energy efficiency (P_{EE}) are in the steady-state regime for the proposed system. Figures 12–15 address the inherent trade-offs between P_{EC} and P_{EE} as a function of the low traffic load ρ. In our numerical discussion, we have used the energy consumption parametric values in the different states of the UE as $\alpha_{\mathrm{SS}} = 3.8\,\mathrm{mW}$, $\alpha_{\mathrm{SL}} = 11.4\,\mathrm{mW}$, $\alpha_{\mathrm{BIM}} = 1060\,\mathrm{mW}$ and $\alpha_{\mathrm{AP}} = 1680\,\mathrm{mW}$ based on results from Huang *et al.* [18].

Figure 12 illustrates the graph of the average energy consumption P_{EC} and the energy efficiency P_{EE} *versus* the low traffic load ρ by varying the values of ξ for $(\nu, \delta, \eta) = (2.5, 1.5, 2)$. Evidently, P_{EC} rises substantially, whereas P_{EE} declines monotonically for increasing values of ρ, which agrees with our intuition. Furthermore,

TABLE 3. Mean and variance of $T_B^{(N)}$ for $(\delta, \eta, \nu) = (2.5, 2.5, 3)$.

	$N = 7$			$N = 12$			$N = 17$		
ρ	$\xi = 1.5$	$\xi = 2.5$	$\xi = 3.5$	$\xi = 1.5$	$\xi = 2.5$	$\xi = 3.5$	$\xi = 1.5$	$\xi = 2.5$	$\xi = 3.5$
0.2	2.40E+05	2.08E+05	1.94E+05	7.50E+08	6.49E+08	6.05E+08	2.34E+12	2.03E+12	1.89E+12
	5.76E+10	**4.31E+10**	**3.75E+10**	**5.63E+17**	**4.21E+17**	**3.66E+17**	**5.50E+24**	**4.11E+24**	**3.57E+24**
0.3	1.20E+04	1.05E+04	9.89E+03	4.92E+06	4.33E+06	4.07E+06	2.03E+09	1.78E+09	1.68E+09
	1.43E+08	**1.10E+08**	**9.78E+07**	**2.42E+13**	**1.87E+13**	**1.66E+13**	**4.11E+18**	**3.17E+18**	**2.81E+18**
0.4	1.56E+03	1.39E+03	1.32E+03	1.52E+05	1.36E+05	1.29E+05	1.49E+07	1.33E+07	1.26E+07
	2.42E+06	**1.92E+06**	**1.73E+06**	**2.32E+10**	**1.84E+10**	**1.66E+10**	**2.21E+14**	**1.76E+14**	**1.58E+14**
0.5	348.2	314.2	299.6286	1.12E+04	1.02E+04	9.69E+03	3.60E+05	3.25E+05	3.10E+05
	1.21E+05	**9.83E+04**	**8.94E+04**	**1.26E+08**	**1.03E+08**	**9.38E+07**	**1.30E+11**	**1.06E+11**	**9.61E+10**
0.6	111.2602	101.5039	97.3227	1.48E+03	1.35E+03	1.30E+03	1.91E+04	1.75E+04	1.68E+04
	1.22E+04	**1.02E+04**	**9.34E+03**	**2.19E+06**	**1.83E+06**	**1.68E+06**	**3.65E+08**	**3.05E+08**	**2.81E+08**
0.7	45.9733	42.3407	40.7839	301.8993	279.1858	269.4514	1.83E+03	1.70E+03	1.64E+03
	2.06E+03	**1.74E+03**	**1.61E+03**	**9.00E+04**	**7.69E+04**	**7.16E+04**	**3.35E+06**	**2.87E+06**	**2.67E+06**
0.8	23.0479	21.3944	20.6858	88.2174	82.4874	80.0317	292.2284	274.058	266.2707
	504.3839	**431.0514**	**401.837**	**7.43E+03**	**6.47E+03**	**6.08E+03**	**8.31E+04**	**7.30E+04**	**6.88E+04**
0.9	13.3863	12.5043	12.1263	34.9151	32.9591	32.1207	74.8419	71.0669	69.4491
	164.5374	**141.7477**	**132.745**	**1.08E+03**	**957.1698**	**906.2598**	**5.02E+03**	**4.50E+03**	**4.29E+03**

TABLE 4. Mean and variance of $T_B^{(N)}$ for $(\eta, \xi, \nu) = (2.5, 1.5, 3)$.

	$N = 7$			$N = 12$			$N = 17$		
ρ	$\delta = 2.5$	$\delta = 3.5$	$\delta = 4.5$	$\delta = 2.5$	$\delta = 3.5$	$\delta = 4.5$	$\delta = 2.5$	$\delta = 3.5$	$\delta = 4.5$
0.2	2.40E+05	2.12E+05	1.97E+05	7.50E+08	6.63E+08	6.15E+08	2.34E+12	2.07E+12	1.92E+12
	5.76E+10	**4.50E+10**	**3.87E+10**	**5.63E+17**	**4.40E+17**	**3.78E+17**	**5.50E+24**	**4.29E+24**	**3.69E+24**
0.3	1.20E+04	1.05E+04	9.64E+03	4.92E+06	4.31E+06	3.97E+06	2.03E+09	1.77E+09	1.63E+09
	1.43E+08	**1.10E+08**	**9.29E+07**	**2.42E+13**	**1.86E+13**	**1.57E+13**	**4.11E+18**	**3.15E+18**	**2.67E+18**
0.4	1.56E+03	1.35E+03	1.24E+03	1.52E+05	1.32E+05	1.21E+05	1.49E+07	1.29E+07	1.19E+07
	2.42E+06	**1.83E+06**	**1.54E+06**	**2.32E+10**	**1.75E+10**	**1.47E+10**	**2.21E+14**	**1.67E+14**	**1.41E+14**
0.5	348.2	301.6857	275.8444	1.12E+04	9.75E+03	8.92E+03	3.60E+05	3.12E+05	2.85E+05
	1.21E+05	**9.06E+04**	**7.57E+04**	**1.26E+08**	**9.50E+07**	**7.95E+07**	**1.30E+11**	**9.74E+10**	**8.15E+10**
0.6	111.2602	96.322	88.023	1.48E+03	1.28E+03	1.18E+03	1.91E+04	1.66E+04	1.52E+04
	1.22E+04	**9.15E+03**	**7.63E+03**	**2.19E+06**	**1.65E+06**	**1.38E+06**	**3.65E+08**	**2.75E+08**	**2.30E+08**
0.7	45.9733	39.8603	36.4642	301.8993	263.0761	241.5077	1.83E+03	1.60E+03	1.47E+03
	2.06E+03	**1.54E+03**	**1.28E+03**	**9.00E+04**	**6.82E+04**	**5.74E+04**	**3.35E+06**	**2.55E+06**	**2.15E+06**
0.8	23.0479	20.0442	18.3754	88.2174	77.5266	71.5873	292.2284	258.0785	239.1064
	504.3839	**376.4137**	**313.7095**	**7.43E+03**	**5.70E+03**	**4.83E+03**	**8.31E+04**	**6.46E+04**	**5.53E+04**
0.9	13.3863	11.6862	10.7416	34.9151	31.0055	28.8335	74.8419	67.1905	62.9398
	164.5374	**122.6517**	**102.2158**	**1.08E+03**	**839.7907**	**718.7028**	**5.02E+03**	**3.99E+03**	**3.48E+03**

an increase in ξ rises the P_{EC}, but reduces the P_{EE} for a fixed ρ. This can be attributed to the fact that as the average duration time $\frac{1}{\xi}$ in the long-sleep state decreases, the UE more frequently switches to the beamforming state, thus allowing more time for the beamforming. As a result, energy consumption P_{EC} increases while energy efficiency P_{EE} decreases.

The trends of P_{EC} and P_{EE} with respect to ρ and ν for the proposed 5G-DRX beamforming mechanism are revealed in Figure 13 by fixing the parameters $(\xi, \delta, \eta) = (2.5, 1.5, 2)$. As anticipated, the average energy

TABLE 5. Mean and variance of $T_B^{(N)}$ for $(\delta, \xi, \nu) = (2.5, 1.5, 3)$.

	$N = 7$			$N = 12$			$N = 17$		
ρ	$\eta = 3$	$\eta = 4$	$\eta = 5$	$\eta = 3$	$\eta = 4$	$\eta = 5$	$\eta = 3$	$\eta = 4$	$\eta = 5$
0.2	2.56E+05	2.89E+05	3.21E+05	8.01E+08	9.03E+08	1.00E+09	2.50E+12	2.82E+12	3.14E+12
	6.57E+10	**8.35E+10**	**1.03E+11**	**6.42E+17**	**8.15E+17**	**1.01E+18**	**6.27E+24**	**7.96E+24**	**9.85E+24**
0.3	1.27E+04	1.41E+04	1.56E+04	5.22E+06	5.82E+06	6.42E+06	2.15E+09	2.40E+09	2.64E+09
	1.61E+08	**2.00E+08**	**2.43E+08**	**2.73E+13**	**3.39E+13**	**4.12E+13**	**4.62E+18**	**5.74E+18**	**6.97E+18**
0.4	1.64E+03	1.81E+03	1.98E+03	1.61E+05	1.77E+05	1.94E+05	1.57E+07	1.73E+07	1.89E+07
	2.69E+06	**3.28E+06**	**3.92E+06**	**2.58E+10**	**3.14E+10**	**3.75E+10**	**2.46E+14**	**2.99E+14**	**3.58E+14**
0.5	365.2	399.2	433.2	1.18E+04	1.29E+04	1.40E+04	3.77E+05	4.12E+05	4.47E+05
	1.33E+05	**1.59E+05**	**1.87E+05**	**1.39E+08**	**1.66E+08**	**1.95E+08**	**1.42E+11**	**1.70E+11**	**2.00E+11**
0.6	116.1383	125.8945	135.6507	1.54E+03	1.67E+03	1.80E+03	1.99E+04	2.16E+04	2.32E+04
	1.34E+04	**1.57E+04**	**1.83E+04**	**2.38E+06**	**2.79E+06**	**3.23E+06**	**3.97E+08**	**4.65E+08**	**5.39E+08**
0.7	47.7896	51.4222	55.0548	313.2561	335.9696	358.6831	1.90E+03	2.04E+03	2.17E+03
	2.23E+03	**2.58E+03**	**2.97E+03**	**9.69E+04**	**1.12E+05**	**1.27E+05**	**3.60E+06**	**4.14E+06**	**4.71E+06**
0.8	23.8746	25.5281	27.1816	91.0824	96.8124	102.5423	301.3136	319.4839	337.6543
	542.4392	**622.6509**	**708.3307**	**7.93E+03**	**8.98E+03**	**1.01E+04**	**8.85E+04**	**9.96E+04**	**1.11E+05**
0.9	13.8274	14.7094	15.5914	35.8932	37.8493	39.8053	76.7294	80.5044	84.2793
	176.163	**200.581**	**226.5551**	**1.15E+03**	**1.28E+03**	**1.43E+03**	**5.28E+03**	**5.84E+03**	**6.43E+03**

TABLE 6. Mean and variance of $T_B^{(N)}$ for $(\delta, \xi, \eta) = (2.5, 1.5, 2.5)$.

	$N = 7$			$N = 12$			$N = 17$		
ρ	$\nu = 3.5$	$\nu = 4.5$	$\nu = 5.5$	$\nu = 3.5$	$\nu = 4.5$	$\nu = 5.5$	$\nu = 3.5$	$\nu = 4.5$	$\nu = 5.5$
0.2	2.50E+05	2.69E+05	2.89E+05	7.81E+08	8.42E+08	9.03E+08	2.44E+12	2.63E+12	2.82E+12
	6.24E+10	7.26E+10	8.35E+10	6.10E+17	7.09E+17	8.15E+17	5.95E+24	6.92E+24	7.97E+24
0.3	1.24E+04	1.33E+04	1.41E+04	5.10E+06	5.47E+06	5.82E+06	2.10E+09	2.25E+09	2.40E+09
	1.54E+08	1.76E+08	2.00E+08	2.60E+13	2.99E+13	3.39E+13	4.41E+18	5.05E+18	5.74E+18
0.4	1.61E+03	1.71E+03	1.81E+03	1.57E+05	1.68E+05	1.77E+05	1.54E+07	1.63E+07	1.73E+07
	2.58E+06	2.92E+06	3.28E+06	2.47E+10	2.81E+10	3.14E+10	2.36E+14	2.67E+14	2.99E+14
0.5	358.4	378.8	399.2	1.16E+04	1.22E+04	1.29E+04	3.70E+05	3.91E+05	4.12E+05
	1.28E+05	1.43E+05	1.59E+05	1.34E+08	1.50E+08	1.66E+08	1.37E+11	1.53E+11	1.70E+11
0.6	114.187	120.0408	125.8945	1.52E+03	1.60E+03	1.67E+03	1.96E+04	2.06E+04	2.16E+04
	1.29E+04	1.43E+04	1.57E+04	2.30E+06	2.55E+06	2.79E+06	3.84E+08	4.24E+08	4.65E+08
0.7	47.0631	49.2426	51.4222	308.7134	322.7503	335.9696	1.87E+03	1.96E+03	2.04E+03
	2.16E+03	2.37E+03	2.58E+03	9.41E+04	1.03E+05	1.12E+05	3.50E+06	3.81E+06	4.14E+06
0.8	23.5439	24.536	25.5281	89.9364	93.4775	96.8124	297.6795	308.5817	319.4839
	526.7885	573.074	621.3281	7.73E+03	8.36E+03	8.98E+03	8.63E+04	9.28E+04	9.96E+04
0.9	13.651	14.1802	14.7094	35.502	36.7108	37.8493	75.9744	78.2394	80.5044
	171.3249	185.3201	199.8754	1.12E+03	1.20E+03	1.28E+03	5.18E+03	5.50E+03	5.84E+03

consumption P_{EC} rises significantly, whereas the energy efficiency, P_{EE}, of the UE declines as the traffic load ρ increases. Another observation from this figure is that as the values of ν increase for a given ρ, the curves of P_{EC} fall off drastically while the curves of P_{EE} rise moderately. This occurs because as the mean dwelling time $\frac{1}{\nu}$ in the beamforming state decreases, the UE transits to a power-saving short sleep state. This results in high energy consumption during beamforming, thus reducing energy efficiency.

Figure 14 depicts how both P_{EC} and P_{EE} vary in the 5G-DRX beamforming mechanism as a function of ρ, for different δ values with specific parameters $(\nu, \xi, \eta) = (2.5, 1, 2)$. We observe from the figure that as ρ increases the energy consumption P_{EC} rises gradually, while the energy efficiency P_{EE} declines sharply for a fixed δ, as expected. One can also conclude that for any given value of ρ, increasing δ leads to a significant rise in P_{EC}, but causes a slight reduction in P_{EE}. This trend occurs because, as the mean time spent in the short-sleep state, $\frac{1}{\delta}$, decreases, the UE promptly transits to the beamforming state. Evidently, this leads to an increase in energy consumption P_{EC} and a decrease in energy efficiency P_{EE} of the UE as expected.

Finally, we analyze the behaviours of both P_{EC} and P_{EE} as functions of both ρ and η while keeping the parameters $(\nu, \delta, \xi) = (2.5, 1.5, 2)$ as depicted in Figure 15 for the 5G-DRX beamforming configuration. As before, the figure shows that P_{EC} rises, while P_{EE} declines as ρ increases, for a fixed value of η. Whereas for any given value of ρ, P_{EE} declines sharply, while P_{EC} rises gradually as the value of η increases. This is because, in the 5G-DRX beamforming state causes the UE to switch more quickly to the long-sleep state. This leads to a reduction in data packet transmission but an increase in energy saving of the UE.

10.5. Time to congestion

We now pay our attention to analyze numerically the behavior of the mean $m_B^{(N)}(1) = \mathrm{E}(T_B^{(N)})$ and variance $\mathrm{Var}(T_B^{(N)})$ for the FPT random variable T_B^N to reach a predefined value N in the waiting line buffer, starting from the beamforming state $n = B$, as derived analytically in Section 8. These metrics offer insights into the data packet congestion levels at the eNB's waiting line buffer for the 5G-DRX wireless communication deployment under investigation.

In Tables 3–6, we present a numerical study of $m_B^{(N)}(1)$ (upper position) and $\mathrm{Var}(T_B^{(N)})$ (lower position) of $T_B^{(N)}$ as a functions of traffic load ρ for three different predefined value N. For each pair of values (ξ, N), the columns corresponding to $\xi = 1.5, 2.5$, and 3.5 in Table 3 show that both indices $m_B^{(N)}(1)$ and $\mathrm{Var}(T_B^{(N)})$ decrease monotonically as ρ increases by choosing $(\delta, \eta, \nu) = (2.5, 2.5, 3)$. Similarly, for a fixed (ρ, N), both descriptors $m_B^{(N)}(1)$ and $\mathrm{Var}(T_B^{(N)})$ decrease as ξ increases as is to be expected. In contrast, when (ρ, ξ) is held constant, both $m_B^{(N)}(1)$ and $\mathrm{Var}(T_B^{(N)})$ decrease drastically as the predefined value N increases. This behavior is consistent with our intuitive expectation, because a higher threshold value N leads to greater values for both the mean and variance of $T_B^{(N)}$.

Table 4 illustrates the effects of ρ, δ, and N on $m_B^{(N)}(1)$ and $\mathrm{Var}(T_B^{(N)})$. For $(\eta, \xi, \nu) = (2.5, 1.5, 3)$ with each fixed pair (δ, N), it can be observed that both $m_B^{(N)}(1)$ and $\mathrm{Var}(T_B^{(N)})$ are decreasing in ρ. Also, it can be see that, for each choice of (ρ, N), the descriptors $m_B^{(N)}(1)$ and $\mathrm{Var}(T_B^{(N)})$ decrease while the values of δ increase. Whereas, for a fixed value of (ρ, δ), both indices $m_B^{(N)}(1)$ and $\mathrm{Var}(T_B^{(N)})$ increase rapidly as the threshold value N grows. These observed trends agree with our intuition. In addition, it can be noticed that the numerical results with respect to δ in Table 4 show a behaviour similar to that of the numerical values relating to ξ in Table 3.

We now analyze the characteristics of the descriptors $m_B^{(N)}(1)$ and $\mathrm{Var}(T_B^{(N)})$ in Table 5 by varying the system parameters ρ, η, and N. From the table, it is seen that for $(\delta, \xi, \nu) = (2.5, 1.5, 3)$ and each fixed pair (η, N), both the mean $m_B^{(N)}(1)$ and the variance $\mathrm{Var}(T_B^{(N)})$ show decreasing trend as ρ increases. On the other side, for each fixed (ρ, N), both $m_B^{(N)}(1)$ and $\mathrm{Var}(T_B^{(N)})$ increase significantly with higher values of η when considering the other parametric values $(\delta, \xi, \nu) = (2.5, 1.5, 3)$ remain constant. Furthermore, for the specified pair of values (ρ, η), it can be inferred from each row of Table 5 that both the average measures $m_B^{(N)}(1)$ and $\mathrm{Var}(T_B^{(N)})$ display an increasing trend as the threshold value N in the waiting line buffer increases, which again fits our intuition quite well.

Lastly, we revisit the effect of the parameters ρ, ν, and N on $m_B^{(N)}(1)$ and $\mathrm{Var}(T_B^{(N)})$ for $(\delta, \xi, \eta) = (2.5, 1.5, 2.5)$. A quick examination of Table 6 reveals that increase in ρ, decreases the values of $m_B^{(N)}(1)$ and $\mathrm{Var}(T_B^{(N)})$ for each fixed pair of (ν, N). On the other side, when the values of ν increase the average measures

$m_B^{(N)}(1)$ and $\mathrm{Var}(T_B^{(N)})$ increase for the fixed values of (ρ, N). Moreover, for the given pair of values (ρ, ν), the table illustrates that both indices $m_B^{(N)}(1)$ and $\mathrm{Var}(T_B^{(N)})$ increase rapidly as the threshold value N increases. These trends clearly meet our intuitive expectations. Here too, it is worth noting that the numerical results relating to ν in Table 6 exhibit a behavior similar to those results with respect to η in Table 5.

11. Conclusion and further directions

In this research article, we proposed a dynamic energy-efficient technique for the UE in the context of LTE DRX beam searching for a 5G mmWave wireless mobile environment to evaluate the performance of the proposed 5G-DRX wireless connectivity in LTE. We utilized a Markovian queueing system and derived analytical results across various UE states under dynamic short and long sleep cycle periods. In the context of real-time applications and practical use cases, we derived explicit closed-form expressions for both transient and steady-state queueing performance metrics, including system throughput, data packet latency, and the average time it takes for data packets to reach congestion in the eNB's buffer. Additionally, we explored the energy-saving potential and energy consumption of the UE during LTE DRX operation in a 5G network. Extensive numerical results were provided to validate the effectiveness of the proposed system.

Our analysis relies on assuming a Poisson arrival process to model LTE DRX for 5G network traffic. This assumption has the advantage of yielding closed-form expressions for both transient and steady-state probabilities, as well as their related performance characteristics. In future work, we plan to incorporate correlated arrival processes, such as Phase-Type and Markovian Arrival Processes. Moreover, we will explore a stochastic game-based approach to analyze energy efficiency across the entire LTE DRX mechanism in 5G network architectures.

Acknowledgments

The authors are grateful to the anonymous referees and associate editor for their critical reading of the manuscript, fruitful suggestions and constructive comments that have improved the presentation and quality of this manuscript.

References

[1] M. Agiwal, A. Roy and N. Saxena, Next generation 5G wireless networks: a comprehensive survey. *IEEE Commun. Surv. Tutor.* **18** (2016) 1617–1655.

[2] M.R.G. Aghdam, B. Rahmani and R. Abdolee, Traffic-based adjustable discontinuous reception mechanism with bounded delay, in 2021 16th Annual Conference on Wireless On-demand Network Systems and Services (WONS 2021), IEEE Xplore, Klosters, Switzerland (2021) 132–137.

[3] G. Anapam, G. Choudhury and S. Dharmaraja, Performance analysis of DRX mechanism using batch arrival vacation queueing system with N-policy in LTE-A networks. *Ann. Telecommun.* **75** (2020) 353–367.

[4] B. Arunsundar, P. Sakthivel and E. Natarajan, Analysis of energy consumption and latency in advanced wireless networks through DRX mechanism. *J. Supercomput.* **76** (2020) 3765–3787.

[5] S. Baek and B.D. Choi, Analysis of discontinuous reception (DRX) with both downlink and uplink packet arrivals in 3GPP LTE, in Proceedings of the 6th International Conference on Queueing Theory and Network Applications (QTNA) (2011) 8–16.

[6] S. Baek and B.D. Choi, Analysis of discontinuous reception with both downlink and uplink packet arrivals in 3GPP LTE. *J. Ind. Manag. Optim.* **8** (2012) 841–860.

[7] P.J. Burke, The output of a queueing system. *Oper. Res.* **4** (1956) 699–704.

[8] Q.H. Choo and B. Conolly, New results in the theory of repeated orders queueing systems. *J. Appl. Probab.* **16** (1979) 631–640.

[9] A. Chydzinski, Time to reach buffer capacity in a BMAP queue. *Stoch. Models* **23** (2007) 195–209.

[10] T. Czachórski, E. Gelenbe, G.S. Kuaban and D. Marek, Transient behaviour of a network router, in 2020 43rd International Conference on Telecommunications and Signal Processing (TSP). IEEE (2020) 246–251.

[11] S. Dharmaraja, A. Aggarwal and R. Sudhesh, Analysis of energy saving in user equipment in LTE-A using stochastic modelling. *Telecommun. Syst.* **80** (2022) 123–140.

[12] I. Dimitriou, Queueing analysis of the DRX power saving mechanism in fault-tolerant 3GPP LTE wireless networks. *Ann. Oper. Res.* **239** (2016) 521–552.

[13] S. Fowler, R.S. Bhamber and A. Mellouk, Analysis of adjustable and fixed DRX mechanism for power saving in LTE/LTE-Advanced, in 2012 IEEE International Conference on Communications (ICC). IEEE (2012) 1964–1969.

[14] S. Fowler, A.O. Shahidullah, M. Osman, J.M. Karlsson and D. Yuan, Analytical evaluation of extended DRX with additional active cycles for light traffic. *Comput. Netw.* **77** (2015) 90–102.

[15] V. Giorno and A.G. Nobile, First-passage times and related moments for continuous-time birth–death chains. *Ric. Mat.* **68** (2019) 629–659.

[16] A. Ghosh, T.A. Timothy, M.C. Cudak, R. Ratasuk, P. Moorut, F.W. Vook, T.S. Rappaport, G.R. MacCartney, S. Sun and S. Nie, Millimeter-wave enhanced local area systems: a high-data-rate approach for future wireless networks. *IEEE J. Sel. Areas Commun.* **32** (2014) 1152–1163.

[17] S. Herreria-Alonso, M. Rodríguez-Pérez, M. Fernández-Veiga and C. López-García, Adaptive DRX scheme to improve energy efficiency in LTE networks with bounded delay. *IEEE J. Sel. Areas Commun.* **33** (2015) 2963–2973.

[18] J. Huang, F. Qian, A. Gerber, Z.M. Mao, S. Sen and O. Spatscheck, A close examination of performance and power characteristics of 4G LTE networks, in Proceedings of the 10th International Conference on Mobile Systems, Applications, and Services (2012) 225–238.

[19] A. Huang, K.H. Lin and H.Y. Wei, Beam-aware cross-layer DRX design for 5G millimeter wave communication system. *IEEE Access* **8** (2020) 77604–77617.

[20] M.T. Kawser, M.R. Islam, K.Z. Islam, M.A. Islam, M.M. Hassan, Z. Ahmed and R. Hasan, Improvement in DRX power saving for non-real-time traffic in LTE. *ETRI J.* **38** (2016) 622–633.

[21] W.M. Kempa, K. Ksiazek and R. Marjasz, On time-dependent queue-size distribution in a model with finite buffer capacity and deterministic multiple vacations with applications to LTE DRX machanism modeling. *IEEE Access* **9** (2021) 148374–148383.

[22] M. Kijima, Markov Processes for Stochastic Modeling. Chapman and Hall, London (1997).

[23] A.T. Koc, S.C. Jha, R. Vannithamby and M. Torlak, Device power saving and latency optimization in LTE-A networks through DRX configuration. *IEEE Trans. Wireless Commun.* **13** (2014) 2614–2625.

[24] B. Krishna Kumar, R. Navaneetha Krishnan, R. Sankar and R. Rukmani, Performance analysis of cognitive wireless retrial queueing networks with admission control for secondary users. *Qual. Technol. Quant. Manag.* **20** (2023) 633–670.

[25] B. Krishna Kumar, R. Sankar, R. Navaneetha Krishnan, R. Rukmani and S. Balaji, Algorithmic analysis of cognitive multichannel retrial network system with finite-source primary users and admission control for secondary users. *Int. J. Commun. Syst.* **38** (2025) e70006.

[26] V.G. Kulkarni, Modeling and Analysis of Stochastic Systems. Chapman and Hall, CRC Press, New York (2016).

[27] S.W. Kwon, J. Hwang, A. Agiwal and H. Kang, Performance analysis of DRX mechanism considering analogue beamforming in millimeter-wave mobile broadband system, in 2014 IEEE GLOBECOM Workshops-Emerging Technologies for 5G Wireless Cellular Networks. IEEE (2014) 802–807.

[28] M. Li and Y.C. Lo, Traffic regulation for power saving in LTE-A networks supporting video-on-demand services, in 2016 Eighth International Conference on Ubiquitous and Future Networks (ICUFN). IEEE (2016) 932–936.

[29] S.H. Lim, S.W. Lee, M. Sohn and B.H. Lee, Queueing analysis of dynamic power management schemes for mobile devices. *IEEE Access* **8** (2020) 97632–97642.

[30] K.H. Lin, H.H. Liu, K.H. Hu, A. Huang and H.Y. Wei, A survey on DRX mechanism: device power saving from LTE and 5G new radio to 6G communication systems. *IEEE Commun. Surv. Tutor.* **25** (2023) 156–183.

[31] D. Liu, C. Wang and L.K. Rasmussen, Discontinuous reception for multiple-beam communication. *IEEE Access* **7** (2019) 46931–46946.

[32] S. Lokesh, J.M. Liang and S.L. Wu, Discontinuous reception based energy-efficient user association for 5G heterogeneous networks. *IEEE Access* **12** (2024) 13634–13647.

[33] M.K. Maheshwari, M. Agiwal, N. Saxena and A. Roy, Directional discontinuous reception (DDRX) for mmWave enabled 5G communications. *IEEE Trans. Mob. Comput.* **18** (2018) 2330–2343.

[34] M.K. Maheshwari, A. Roy and N. Saxena, DRX over LAA-LTE-a new design and analysis based on semi-Markov model. *IEEE Trans. Mob. Comput.* **18** (2019) 276–289.

[35] M.K. Maheshwari, E. Rastogi, A. Roy, N. Saxena and D.R. Shin, DRX in NR unlicensed for B5G wireless: modeling and analysis. *IEEE Trans. Mob. Comput.* **22** (2023) 5184–5197.

[36] M.K. Maheshwari, M. Agiwal and A. Rashid Masud, Analytical modeling for signaling-based DRX in 5G communication. *ETT* **32** (2020) e4125.

[37] V. Mancuso and S. Alouf, Analysis of power saving with continuous connectivity. *Comput. Netw.* **56** (2012) 2481–2493.

[38] Y. Mehmood, L. Zhang and A. Förster, Power consumption modeling of discontinuous reception for cellular machine type communications. *Sensors* **19** (2019) 617.

[39] M.L. Memon, M.K. Maheshwari, N. Saxena, A. Roy and D.R. Shin, Artificial intelligence-based discontinuous reception for energy saving in 5G networks. *Electronics* **8** (2019) 1–17.

[40] S.J. Park and M.Y. Choi, Analytic expression of the probability density function for the first-passage time in birth-death processes. *Chaos Soliton Fract.* **186** (2024) 115307.

[41] N.R. Philip and B. Malarkodi, Extended hybrid directional DRX with auxiliary active cycles for light traffic in 5G networks. *ETT* **30** (2019) e3552.

[42] N.R. Philip and B. Malarkodi, Beam-aware energy harvesting discontinuous reception in machine-to-machine millimeter-wave 5G communications. *Int. J. Commun. Syst.* **33** (2020) e4567.

[43] N.U. Prabhu, Foundations of Queueing Theory. Vol. 7. Springer Science & Business Media, New York (2012).

[44] K. Priyanka and S. Dharmaraja, Stochastic modeling for energy efficiency in modified directional discontinuous reception for LTE-5G networks. *Int. J. Commun. Syst.* **36** (2023) e5434.

[45] B. Rahmani, M.R. Ghavidel Aghdam and R. Abdolee, Energy efficient discontinuous reception strategy in LTE and beyond using an adaptive packet queuing technique. *IET Commun.* **14** (2020) 3247–3255.

[46] H. Ramazanali and A. Vinel, Performance evaluation of LTE/LTE-A DRX: a Markovian approach. *IEEE Internet Things J.* **3** (2015) 386–397.

[47] H. Ramazanali and A. Vinel, Mean queuing delay in LTE DRX. *IEEE Wirel. Commun. Lett.* **5** (2016) 444–447.

[48] E. Rastogi, M.K. Maheshwari and A. Rastogi, Performance analysis of user power consumption in NR-Unlicensed DRX. *J. Supercomput.* **81** (2025) 329.

[49] W. Roh, J.Y. Seol, J. Park, B. Lee, J. Lee, Y. Kim, J. Cho, K. Cheun and F. Aryanfar, Millimeter-wave beamforming as an enabling technology for 5G cellular communications: theoretical feasibility and prototype results. *IEEE Commun. Mag.* **52** (2014) 106–113.

[50] D.E. Ruiz-Guirola, C.A. Rodríguez-Lopez, O.L. Lopez, S. Montejo-Sanchez, V.A. Reguera and M. Latva-aho, Discontinuous reception with adjustable inactivity timer for iIoT. *IEEE Trans. Ind. Inform.* **21** (2025) 574–583.

[51] M.M. Sallam, H.B. Nafea and F.W. Zaki, Comparative study of power saving and delay in LTE DRX, directional-DRX and hybrid-directional DRX. *WPC* **98** (2018) 3299–3317.

[52] T.L. Saaty, Time-dependent solution of the many-server Poisson queue. *Oper. Res.* **8** (1960) 755–772.

[53] M.M. Sallam, F.W. Zaki, M.M. Ashour and H.B. Nafea, Discontinuous reception sleep mode based on beam training procedure in 5G mm Wave communication systems. *EURASIP J. Wirel. Commun. Netw.* **2025** (2025) 1–48.

[54] J.F. Shortle, J.M. Thompson, D. Gross and C.M. Harris, Fundamentals of Queueing Theory. John Wiley and Sons Inc, New York (2018).

[55] O. Shurdi, A. Rakipi and A. Lala, Power saving techniques in 5G technology for multiple-beam communications. *J. Commun. Softw. Syst.* **19** (2023) 168–177.

[56] S. Sur, I. Pefkianakis, X. Zhang and K.H. Kim, Towards scalable and ubiquitous millimeter-wave wireless networks, in Proceedings of the 24th Annual International Conference on Mobile Computing and Networking (2018) 257–271.

[57] H.C. Tijms, Stochastic Models: An Algorithmic Approach. John Wiley and Sons, Chichester (1994).

[58] L.P. Tung, Y.D. Lin, Y.H. Kuo, Y.C. Lai and K.M. Sivalingam, Reducing power consumption in LTE data scheduling with the constraints of channel condition and QoS. *Comput. Netw.* **75** (2014) 149–159.

[59] S.R. Yang and Y.B. Lin, Modeling UMTS discontinuous reception mechanism. *IEEE Trans. Wirel. Commun.* **4** (2005) 312–319.

[60] S.R. Yang, S.Y. Yan and H.N. Hung, Modeling UMTS power saving with bursty packet data traffic. *IEEE Trans. Mob. Comput.* **6** (2007) 1398–1409.

[61] Y. Zhang, S. Jin and W. Yue, An enhanced energy saving strategy for an active DRX in LTE wireless networks. *Int. J. Innov. Comput. Inf. Control* **9** (2013) 4373–4387.

[62] L. Zhou, H. Xu, H. Tian, Y. Gao, L. Du and L. Chen, Performance analysis of power saving mechanism with adjustable DRX cycles in 3GPP LTE, in 2008 IEEE 68th Vehicular Technology Conference. IEEE (2008) 1–5.

[63] K. Zhou, N. Nikaein and T. Spyropoulos, LTE/LTE-A discontinuous reception modeling for machine type communications. *IEEE Wirel. Commun. Lett.* **2** (2012) 102–105.

[64] F. Zhu, Y. Wu and Z. Niu, Delay analysis for sleep-based power saving mechanisms with downlink and uplink traffic. *IEEE Commun. Lett.* **13** (2009) 615–617.

Appendix A. Proof of $|H^*(s)| < 1$

Using (3.28), we have

$$H^*(s) = \frac{\nu\delta}{(\lambda+\nu+\eta-\delta)}\left[\frac{1}{s+\delta} - \frac{1}{s+\lambda+\nu+\eta}\right] + \frac{\eta\xi}{(\lambda+\nu+\eta-\xi)}\left[\frac{1}{s+\xi} - \frac{1}{s+\lambda+\nu+\eta}\right]$$
$$+ \frac{\delta\lambda}{(\lambda+\nu+\eta-\delta)}\left[\frac{1}{s+\delta} - \frac{1}{(s+\lambda+\nu+\eta)}\right]\left[\frac{(s+\lambda+\mu) - \sqrt{(s+\lambda+\mu)^2 - 4\lambda\mu}}{2\lambda}\right]$$
$$H^*(s) = \frac{\nu\delta}{(s+\delta)(s+\lambda+\nu+\eta)} + \frac{\eta\xi}{(s+\xi)(s+\lambda+\nu+\eta)} + \frac{\lambda\delta}{(s+\delta)(s+\lambda+\nu+\eta)}$$
$$\times \left[\frac{(s+\lambda+\mu) - \sqrt{(s+\lambda+\mu)^2 - 4\lambda\mu}}{2\lambda}\right].$$

Since $\frac{(s+\lambda+\mu)-\sqrt{(s+\lambda+\mu)^2-4\lambda\mu}}{2\lambda} < 1$ (see [52], and choose $s > 0$, to be sufficiently large so that

$$H^*(s) < \frac{\nu\delta}{(s+\delta)(s+\lambda+\nu+\eta)} + \frac{\eta\xi}{(s+\xi)(s+\lambda+\nu+\eta)} + \frac{\lambda\delta}{(s+\delta)(s+\lambda+\nu+\eta)}$$
$$= \frac{\delta(\lambda+\nu)(s+\xi)+\eta\xi(s+\delta)}{(s+\delta)(s+\xi)(s+\lambda+\nu+\eta)}.$$

Assume, $\frac{\delta(\lambda+\nu)(s+\xi)+\eta\xi(s+\delta)}{(s+\delta)(s+\xi)(s+\lambda+\nu+\eta)} > 1, \Rightarrow \delta(\lambda+\nu)(s+\xi)+\eta\xi(s+\delta) > (s+\delta)(s+\xi)(s+\lambda+\nu+\eta)$.

Upon simplifying the above inequality yields $s^2(s+\lambda+\nu+\eta) + (\xi s^2 + \lambda\xi s + \nu\xi s) + (\delta s^2 + \eta\delta s) + \delta\xi s < 0$ which is infeasible.

Consequently,

$$\frac{\delta(\lambda+\nu)(s+\xi)+\eta\xi(s+\delta)}{(s+\delta)(s+\xi)(s+\lambda+\nu+\eta)} < 1.$$

Hence, it follows that $|H^*(s)| < 1$ for $s > 0$. Moreover, it is observed that $\lim_{s\to 0} H^*(s) = 1$ for $\lambda < \mu$.

Appendix B. Truncation level K

For numerical purpose, an appropriate truncation level K must be selected for the infinite series of convoluted functions in (3.29). To truncate this series, K is chosen such that $\sum_{n=K+1}^{\infty} H^{©(n)}(t) \approx 0$. It is observed that the sequence $\{H^{©(n)}(t)\}_{n=0}^{\infty}$ is positive, monotonically decreasing and satisfies the ratio convergence test. That is, define

$R = \sup_n \frac{H^{©(n+1)}(t)}{H^{©(n)}(t)}$ and if $R < 1$, then $\sum_{n=K+1}^{\infty} H^{©(n)}(t) \leq \frac{R^{K+1}}{1-R} H^{©(0)}(t) < \epsilon$, truncation error. But $H^{©(0)}(t) = 1$, thereby $R^{K+1} < \epsilon(1-R)$.

So that

$$(K+1) < \frac{log(\epsilon(1-R))}{logR} \quad \Rightarrow \quad K < \frac{log(\epsilon(1-R))}{logR} - 1.$$

Our numerical results indicate that selecting $K \sim 12 - 17$ is adequate for $\epsilon = 10^{-6}$ and $R < 0.5$.